2

(NASA-CR-127765) UNSTEADY FLOW THROUGH COMPRESSOR STAGES E. Alzner, et al (Advanced Technology Labs., Inc.) Dec. 1971 72 p

N72-29227

CSCL 20D G3/12

Unclas 15906

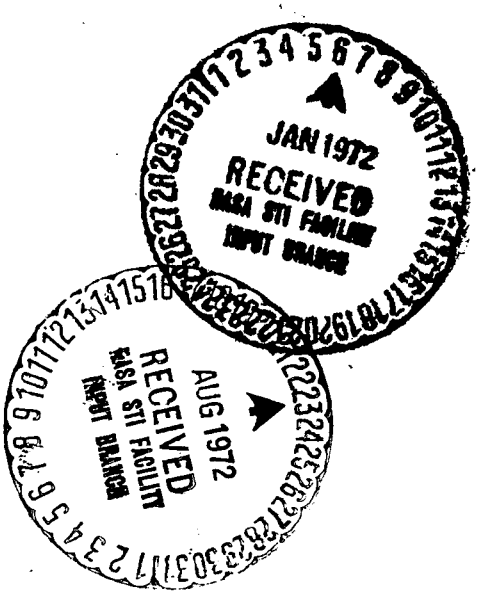

ADVANCED TECHNOLOGY LABORATORIES, INC.

DECEMBER 1971

ATL TR 168

UNSTEADY FLOW THROUGH COMPRESSOR STAGES

By

Edgar Alzner and John Erdos

PREPARED FOR

NASA HEADQUARTERS
WASHINGTON, D. C.

BY

ADVANCED TECHNOLOGY LABORATORIES, INC.
400 Jericho Turnpike
Jericho, N. Y. 11753

INDEX

LIST OF FIGURES

LIST OF FIGURES (Continued)

I. INTRODUCTION

The introduction of large bypass-ratio turbofan engine designs has significantly reduced jet exhaust noise (which is primarily related to mixing of the exhaust stream with the surrounding atmosphere) and thereby focussed attention on the fan and compressor as predominant contributors to the acoustic signature of turbofan engines during aircraft landing approach[1]. The use of inlet noise suppression devices holds promise for attenuating the acoustic output of large fans (cf., Reference 2). It is, however, evident that optimization of the trade-offs between performance and acoustic output in the preliminary design of advanced engines is dependent upon more complete understanding of the aerodynamic sources of the acoustic signals and the factors affecting their propagation through the gaseous stream injested by the engine. In point of fact, performance requirements[3] tend to drive fan designs toward very small hub to tip ratios, transonic or supersonic tip speeds, and high blade loading, all of which are in direct contradiction to the assumptions underlying most previous analyses of non-steady aerodynamics of rotors and rotor-stator interactions (cf. References 4-8).

The present research has resulted in a powerful method of analysis of non-steady flow fields associated with rotor-stator

interaction. This method, which is capable of treating heavily loaded blades operating at transonic and supersonic speeds, including generation of imbedded shock waves, involves numerical solution of the complete, nonlinear partial differential equations governing the flow. The generation and propagation of finite amplitude, nonlinear acoustic waves is therefore an inherent part of the flow field solutions thereby obtained. Furthermore, the technique developed is also applicable to analysis of rotor performance in spatially distorted inlet flows and the related acoustic response.

II. TECHNICAL APPROACH

A. Description of the problem. Turbo-machinery offers a host of aerodynamic sources of non-steady flows; the frequencies at which the resulting flow patterns are emitted encompass the acoustic range giving rise to a noise pattern that is characteristic of the particular design and operating conditions. The sources of acoustic signals range from turbulent fluctuations in the boundary layers and exhaust stream to the interaction of adjacent rotating and stationary blade rows in the compressor and turbine. The present study has been specifically devoted to rotor-stator blade row interactions in a fan or compressor.

Although the flow about a rotor is steady in a rotating frame of reference, it presents a periodic field in a fixed (stationary) reference frame. This fact has been exploited in the analysis of noise generation by an isolated rotor[6], and underlies the classical rotor-stator interaction theory of Kemp and Sears[7]. However, the previous analyses (References 4-8) consistently employ the assumption of small disturbances in some sense to permit use of a linear governing equation. In the case of incompressible flow about thin, lightly loaded blades the physical justification of the assumption is clear; however as the blade loading is increased and tip speeds become transonic or supersonic, due to the performance requirements of advanced engines,

the utility of solutions of the linearized problem becomes less evident. Finally, the occurrence of shock waves clearly invalidates the assumption of continuous, isentropic flow inherent in the previous work.

In the case of supersonic tip speeds a vivid description of the nature of the radiated acoustic energy can be made by noting that it is analogous to a continuous train of sonic booms being emitted by the rotating fan blades. This analogy also proves useful in describing the mechanism by which the radiated energy decays in distance (or time) due to destructive interference between the successive waves. It is, however, a clearly nonlinear phenomenon in so far as the waves have finite amplitude (e.g., as long as they must be identified as shock waves rather than acoustic waves).

Although the use of models based on linear equations does offer certain appeal, such as the ability to superimpose solutions and thereby separate the contributions of blade camber and thickness, for example[5,6,7], they do not appear adequate under conditions characteristic of advanced fan and/or compressor designs. Therefore, a finite-difference technique generally attributed to Lax and Wendroff [9] was employed in the present study to develop a method of solution of the complete nonlinear partial differential equations and boundary conditions

governing the inviscid flow through adjacent rotating and stationary blade rows. The mechanism of generation and propagation of acoustic signals is therefore an inherent aspect of the numerical solution. The additional consideration of boundary layer and viscous wakes, for example, will allow the salient effects of viscous and inviscid nonuniformities to be individually identified through numerical studies with important implications relative to scaling of acoustic tests and full-scale fan/compressor design.

Description of flow field generated by a rotor-stator combination having an unequal number of blades, or that generated by an isolated rotor operating in a circumferentially distorted inlet flow, in general requires consideration of the entire flow annulus. In certain cases having particular symmetric features it is possible to consider only a fraction of the annulus. Only in the limiting case of undistorted inlet flow and equal blading can the solution of a single blade-to-blade passage at any particular instant be applied to description of the entire annulus at the same instant. However, in the present study it is shown that by developing the appropriate phase relationships a solution for the entire annulus can be constructed by consideration of all combinations of rotor-stator configurations occurring in a single blade-to-blade passage during a fraction of a complete rotation of the fan or compressor wheel. A unique method for applying sequentially

the boundary conditions on the blade-to-blade passage in accordance with the phase relationships is developed. The technique not only economizes the computer requirements of the two dimensional (viz., on a cylindrical surface through the fan or compressor) solutions obtained in the present study, but also renders the extension to three dimensional (viz., in a sector of the annulus) problems tractable from the viewpoint of computer storage and time requirements.

B. Governing equations and finite-difference solution. The inviscid, compressible flow through the fan or compressor is governed by the standard conservation laws for mass and energy, and the non-steady form of the Euler equations. Mathematically, the set forms a hyperbolic system of four partial differential equations that can be solved as an initial value problem. The explicit finite-difference technique generally attributed to Lax and Wendroff[9] offers an algorithm for numerical solution of the system of equations that is more easily implemented than the three dimensional method of characteristics, has second order accuracy in space and time, and can describe imbedded shocks (subject to the influence of an appropriate "numerical viscosity"). The details of the particular version of the method employed is described in Reference (10).

Implementation of the finite-difference algorithm and the

boundary point routines is facilitated by transforming the regions to be considered, shown in Figure (1a), into a series of square domains shown in Figure (1b), that span the blade-to-blade passages from surface to surface and from leading to trailing edge, and extend in the present study, far upstream and downstream of the two blade rows. The resulting system of equations after transformation and suitable non-dimensionalization (i.e., with respect to the free stream speed of sound and pressure) can be expressed as:

Continuity:

$$\frac{\partial \rho}{\partial \tau} + A \frac{\partial}{\partial \sigma} (\rho u) + B \frac{\partial}{\partial \nu} (\rho v) + D_1 = 0 \qquad (1)$$

Energy:

$$\frac{\partial \rho E}{\partial \tau} + A \frac{\partial}{\partial \sigma} (\rho u H) + B \frac{\partial}{\partial \nu} (\rho v H) + D_2 = 0 \qquad (2)$$

σ-Momentum:

$$\frac{\partial \rho u}{\partial \tau} + A \frac{\partial}{\partial \sigma} (\rho u^2 + p) + B \frac{\partial}{\partial \nu} (\rho u v) + D_3 = 0 \qquad (3)$$

ν-Momentum:

$$\frac{\partial \rho v}{\partial \tau} + A \frac{\partial}{\partial \sigma} (\rho u v) + B \frac{\partial}{\partial \nu} (\rho v^2 + p) + D_4 = 0 \qquad (4)$$

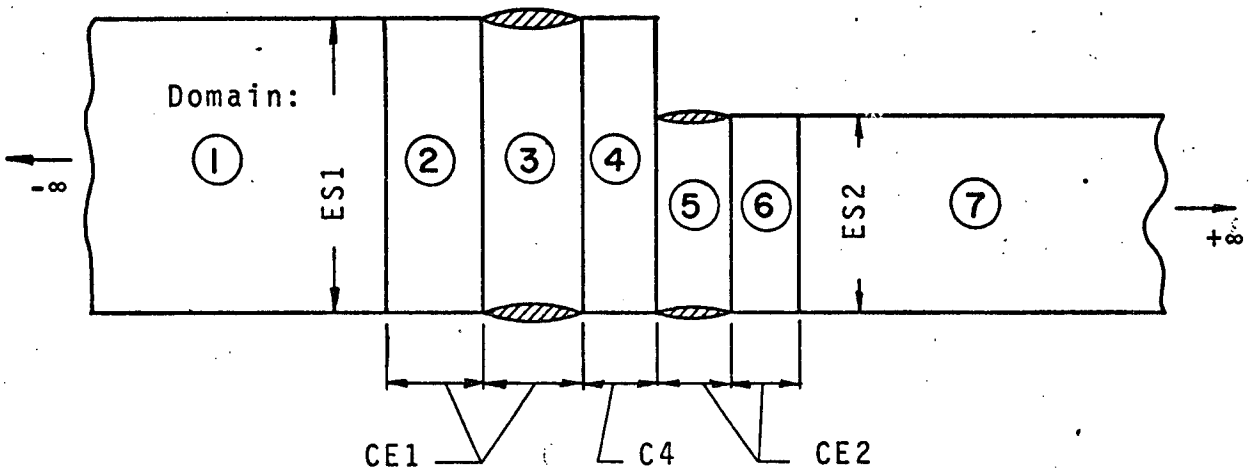

(a) Physical Domains

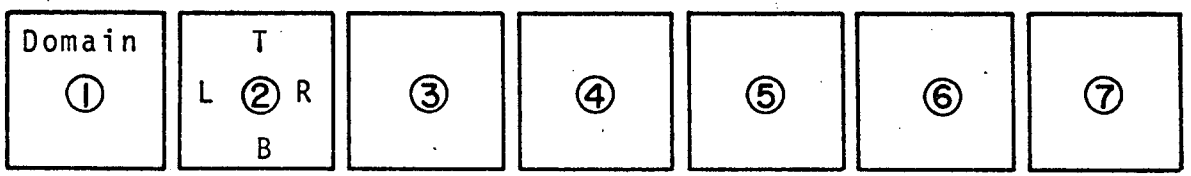

(b) Transformed Square Domains

FIGURE 1. TYPICAL PHYSICAL AND TRANSFORMED DOMAINS FOR A COMPRESSOR STAGE.

where τ is the non-dimensional time, u and v are the velocity components in the Cartesian system, ρ is the density, p is the pressure, H is the total enthalpy and E is the total energy (i.e., $E=H-p/\rho$).

The values of A, B, and D_1 through D_4 in the various domains are given below:

Domain / Coefficient	1	2	3	4	5	6	7
A	σ	1	1	C_δ	C_α	C_α	$(1-\sigma)\ C_\alpha$
B	C_β	C_β	$\frac{C_s}{y_\nu}$	C_β	$\frac{C_s}{y_\nu}$	C_γ	C_γ

where

$$C_\alpha = C_s/C_r$$
$$C_\beta = C_s/S_s$$
$$C_\gamma = C_s/S_r$$
$$C_\delta = C_s/C_4$$

C and S refer to blade chord and pitch respectively, while sub-

scripts s and r denote stator and rotor. C_4 is the inter-blade row gap. In addition y_ν refers to the peripheral span of the blade-to-blade passage, i.e., $y_\nu = y_u - y_\ell$. Then for domains 3 and 5

$$D_1 = - A \frac{y_\sigma}{y_\nu} \frac{\partial}{\partial \nu} (\rho u) + \frac{y_\tau}{y_\nu} \frac{\partial}{\partial \nu} (\rho) \tag{5}$$

$$D_2 = - A \frac{y_\sigma}{y_\nu} \frac{\partial}{\partial \nu} (\rho u H) + \frac{y_\tau}{y_\nu} \frac{\partial}{\partial \nu} (\rho E) \tag{6}$$

$$D_3 = - A \frac{y_\sigma}{y_\nu} \frac{\partial}{\partial \nu} (\rho u^2 + p) + \frac{y_\tau}{y_\nu} \frac{\partial}{\partial \nu} (\rho u) \tag{7}$$

$$D_4 = - A \frac{y_\sigma}{y_\nu} \frac{\partial}{\partial \nu} (\rho u v) + \frac{y_\tau}{y_\nu} \frac{\partial}{\partial \nu} (\rho v) \tag{8}$$

while for domains 1, 2, 4, 6 and 7

$$D_1 = D_2 = D_3 = D_4 = 0 \tag{9}$$

An exponential stretching of the axial coordinate is employed in domains 1 and 7:

$$\sigma = e^{x/C_s} \quad \text{in } 1 \tag{10}$$

$$\sigma = 1 - e^{-x/C_r} \quad \text{in } 7 \tag{11}$$

while in all other domains $\sigma = x/C$. In domains 3 and 5 (the blade rows) the transverse coordinate is linearly scaled to span the blade-to-blade passage:

$$\nu = \frac{y-y_\ell}{y_u-y_\ell} \quad . \tag{12}$$

while in all other domains $\nu = y/S$.

Each of the computational domains is divided into a rectangular grid of fixed mesh size $\Delta\sigma$ by $\Delta\nu$. The spatial derivatives in Equations (1) to (4) are replaced by centered difference formulas of second order accuracy. Second order accuracy in the time derivative is obtained by a two-step procedure described in References (9) and (10).

C. Boundary conditions. The four types of boundaries which will be encountered in the current calculation domains, illustrated in Figure (1), are

(1) The solid blade surfaces indicated as T for top and B for bottom.

(2) The horizontal surfaces extending upstream of the leading blades, downstream of the trailing blades and between the two sets of blades, again indicated as T for top and B for bottom.

(3) The inflow boundary indicated as L.

(4) The outflow boundary indicated as R.

All spatial boundary conditions must be specified so that the problem is properly posed and so that the computation can march ahead in time at all grid points. Statement of the boundary conditions is facilitated by separating the computational field into seven (7) domains as discussed earlier.

Solid Blade Surfaces At the blade surfaces adjusted by a displacement thickness to account for the boundary layer, which will be discussed later, the boundary condition is that the surface is impermeable. It is noted that while the blade surface itself may be translating, additional motion of the effective surface can take place due to non-steady displacement thickness fluctuations. The normal pressure gradient is determined from the normal momentum equation at the wall; the normal gradients of the remaining variables are obtained from non-centered finite difference approximations. The transformed normal momentum equation to be used for evaluating the pressure gradient at a blade surface in domains 3 and 5 is:

$$\frac{\partial p}{\partial \nu} = \left[\frac{y_\nu}{(\frac{C}{S})^2 + (y_\sigma)^2}\right]\left[y_\sigma p_\sigma - \rho\left[u\left(y_{\sigma\sigma}u + \frac{C}{C_s}(y_{\tau\sigma} + y_{\sigma\tau})\right) + (\frac{C}{C_s})^2 y_{\tau\tau}\right]\right] \quad (13)$$

where

$$C = C_s \quad \text{in domain 3}$$
$$S = S_s$$

$$C = C_r \quad \text{in domain 5}$$
$$S = S_r$$

This equation makes use of the fact that the transformed velocity component

$$B = \frac{d\nu}{dt} = \left(\frac{C_s}{a_\infty} V - y_\sigma u - y_\tau\right)/y_\nu \tag{14}$$

at the surface, including the unsteady motion of the surface is zero and flow is tangential relative to the surface. The derivatives y_σ, $y_{\sigma\sigma}$, $y_{\sigma\tau}$ and $y_{\tau\sigma}$ are evaluated by determining the displacement thickness at each point and then forming these derivatives from coordinates equal to surface plus displacement thickness.

Non-Solid Surface Boundary Conditions In order to clearly describe the application of the boundary conditions in the present analysis it is useful to clarify the discussion by introducing several rotating devices that illustrate certain general concepts with minimal complexity of the geometric configuration.

First, consider a symmetric three bladed rotor developed into a cascade as shown in Figure (2).

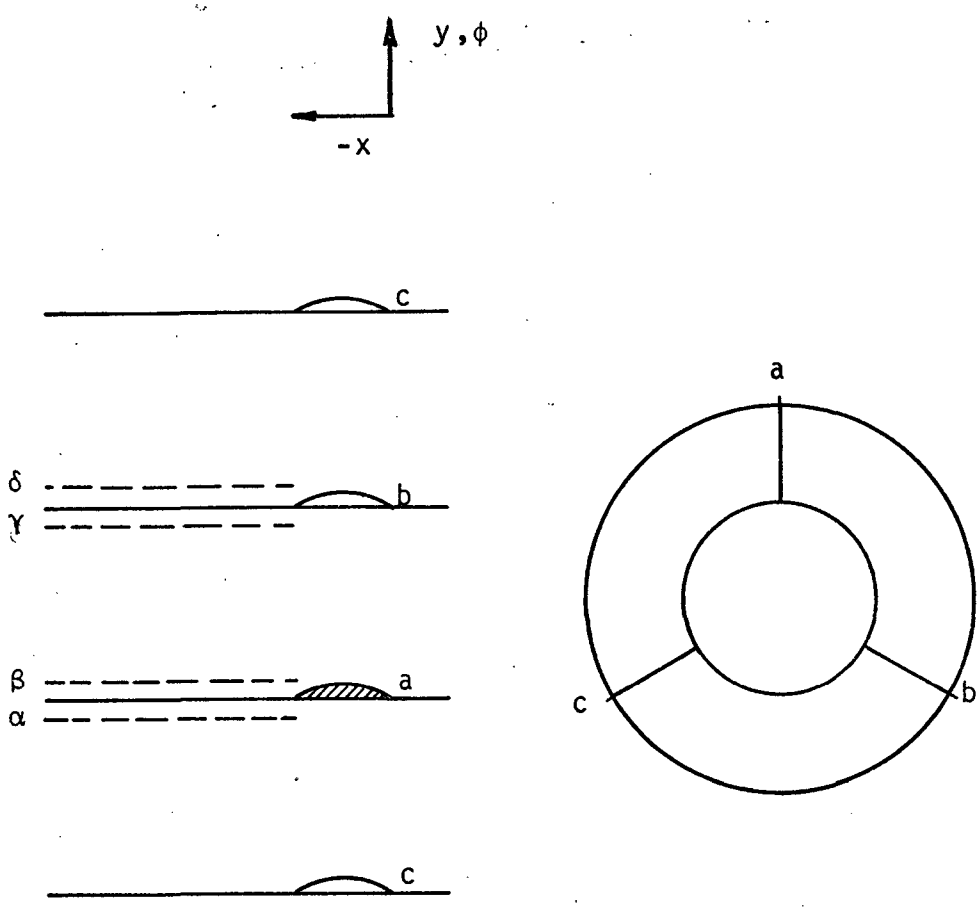

FIGURE 2. ISOLATED BLADE ROW.

Let control surfaces* be drawn from the blade leading and trailing edges to ±∞. By considering both the cascade and end view of the blade row and using a reference frame fixed to the blades it is clear that the flow field in each of the three passages is identical. That is, the flow anywhere on line δ is identical to the flow at corresponding points on

*These control surfaces are, in general, not coincident with streamlines but are perpendicular to the cascade; flow can cross them and disturbances can propagate along and across them.

line β and similarly for line α and γ. A similar agrument also applies to points in the flow field downstream of the blades.

Next consider the system composed of a rotor and stator each having the same number of blades; specifically, consider 3 blades each as shown in Figure (3a).

When the blades are aligned, say at time t_0; as shown in Figure (3a), it is clear that, because symmetry produces identical flow channels, the flow along and through the control surfaces extending from x and between leading and trailing edges is the same in each "passage"; i.e., all influences with respect to corresponding points in the respective "passages" are necessarily the same. For a different relative position, say at some later time $t_0 + \Delta t$ for example, see Figure (3b), the noted symmetry persists since the geometry of respective "passages" is the same and again the flow through the respective control volumes is identical. The same conclusion as above is also reached regarding the equivalence of lines α with γ and δ with β. The same argument again can be applied to the flow field between the two blade rows and also downstream of the second blade row.

It is to be noted that due to the repetition of identical configurations with identical flows it is clear that only one pas-

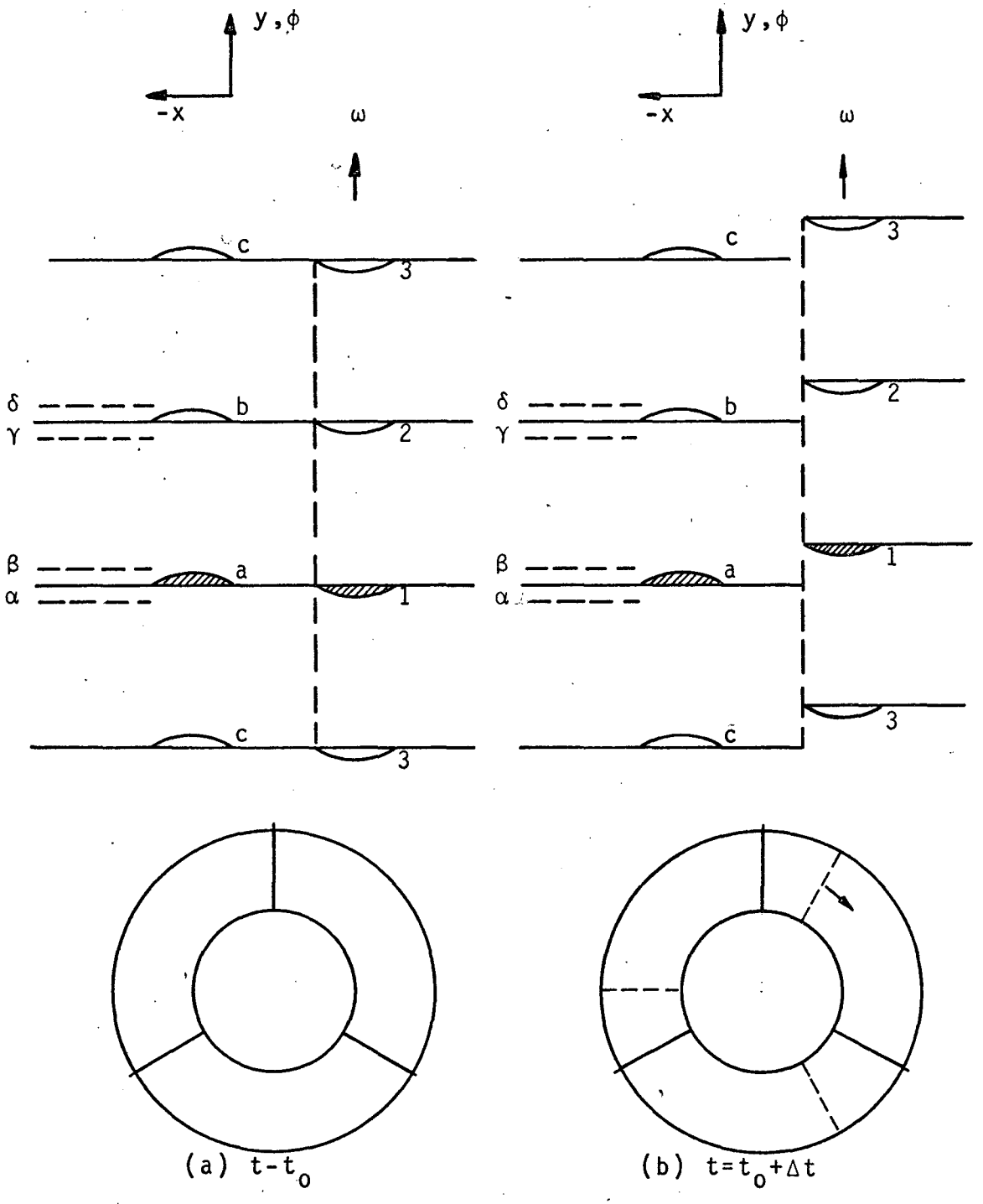

FIGURE 3. COMPRESSOR STAGE WITH EQUAL NUMBER OF BLADES IN STATOR AND ROTOR (N=3, M=3).

sage of each, namely the first blade row, say the stator, and the second blade row, say the rotor, need be computed in order to determine the flow field in the whole periphery of the stage. As a consequence of the equivalence of the corresponding dashed lines, it is also clear that the boundary values, say on line δ, can be specified by equating them to the currently computed values at corresponding points, in this case on line β, to define the boundary conditions for the control volume being computed. Similar reasoning is applied to lines γ and α respectively and to corresponding horizontal boundaries between and downstream of the blades.

It is not obvious that the case of <u>unequal</u> number of blades in stator and rotor can be treated analogously; however, the following detailed explanation is intended to demonstrate clearly that the above techniques for specifying boundary conditions on a single passage can be extended to this case by introduction of a phase shift. In this regard a pair of blade rows, shown in Figure(4a) and (4b) portray the configuration of a 3 bladed stator followed by a 4 bladed rotor which will be used to demonstrate the unequal spacing techniques.

The underlying assumption here is that the conditions very far upstream and downstream ($x \to \pm\infty$) of the stage are uniform and steady, and that the nonsteady flow in the vicinity of

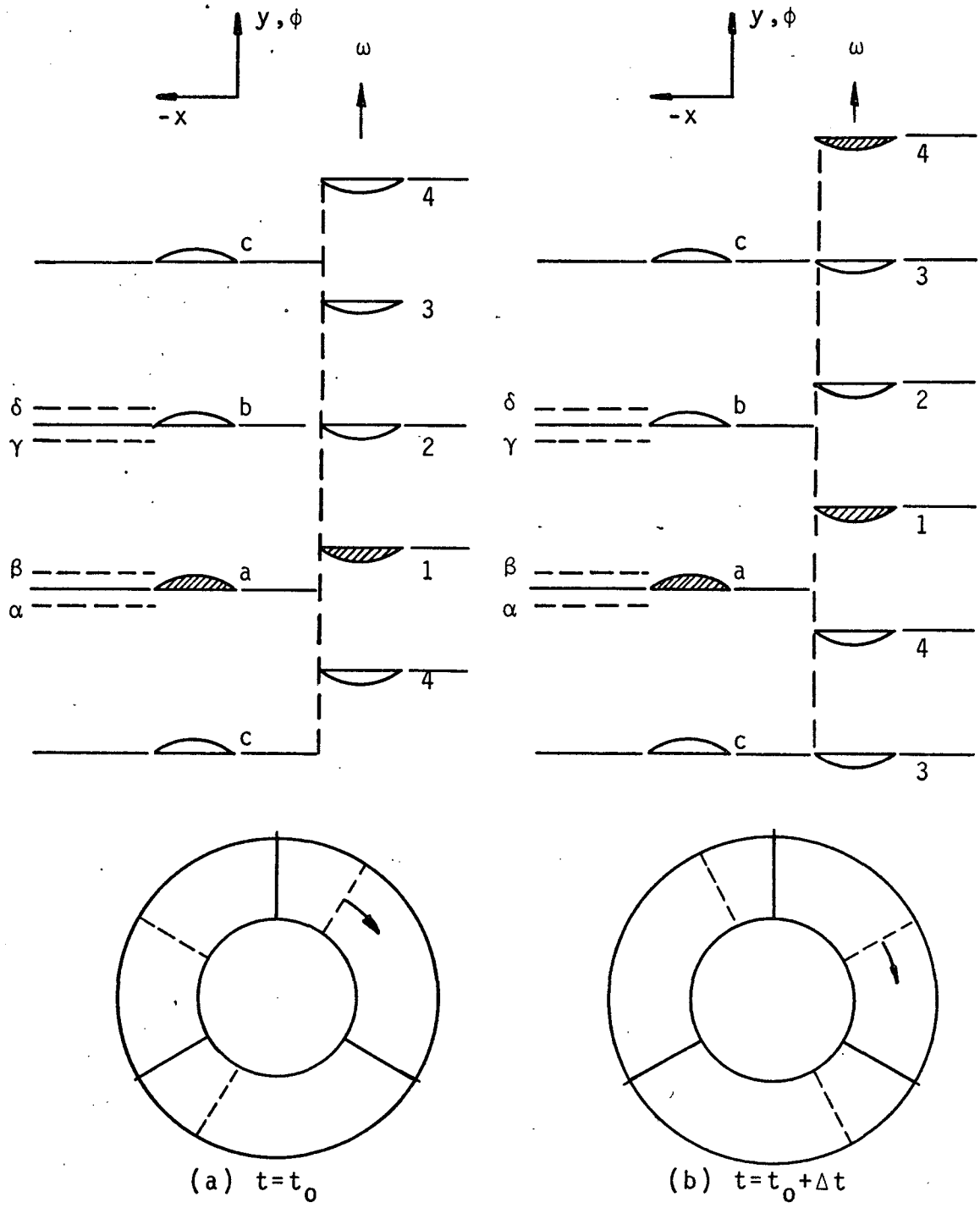

FIGURE 4. COMPRESSOR STAGE WITH UNEQUAL NUMBER OF BLADES IN STATOR AND ROTOR (N=3, M=4).

the stage is periodic in time (i.e., stable). The first question that arises is whether the starting process associated with an arbitrary set of initial conditions does indeed lead to an asymptotically periodic solution. It is most useful to next pictorially describe the actual physical starting process for a system of blade rows set into motion impulsively. This is done for the configuration introduced above with both the rotational speed and free stream velocity subsonic. Figures (5a) to (5m) show the development of disturbance waves thus generated. Only those waves generated when a blade of the rotor is aligned with a blade of the stator are portrayed in these figures and then only a portion of each wave, extending a distance x_w, as shown in Figure (4c), are shown for clarity. One complete revolution of the rotor, an angle of rotation of 2π, is represented over 12 intervals. The time increment for each interval is

$$\Delta t = \frac{2\pi}{NM\omega} = \frac{2\pi}{12\ \omega} \tag{15}$$

where N is the number of blades in the stator, M is the number of blades in the rotor and ω is the rotational speed. The corresponding angular change for each Δt is

$$\Delta\phi = \frac{2\pi}{NM} = \frac{2\pi}{12} \tag{16}$$

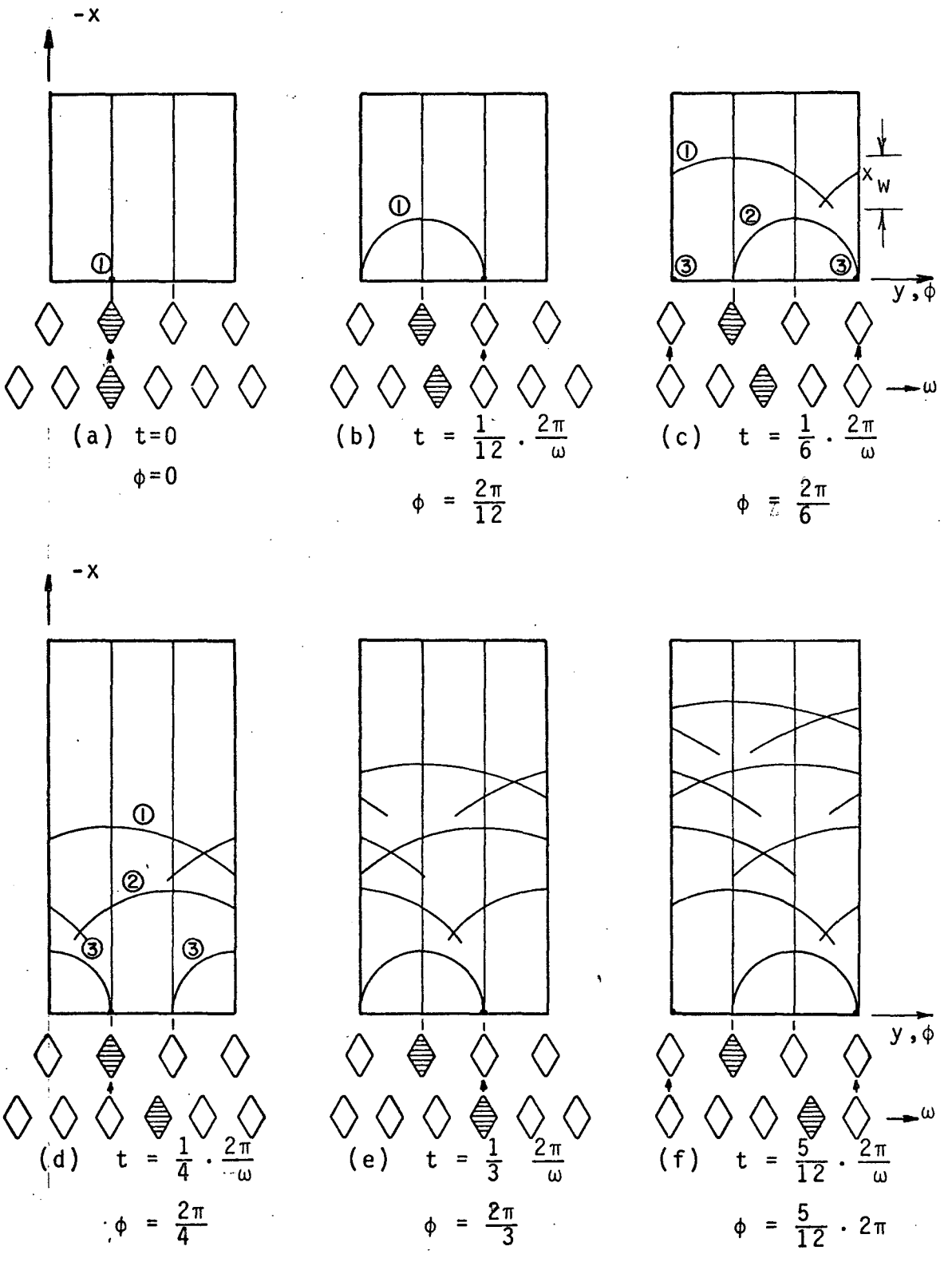

FIGURE 5. STARTING PROCESS SHOWING DEVELOPMENT OF DISTURBANCE WAVES FORMED WHEN BLADES ARE ALIGNED (ACTUAL SOLUTION)

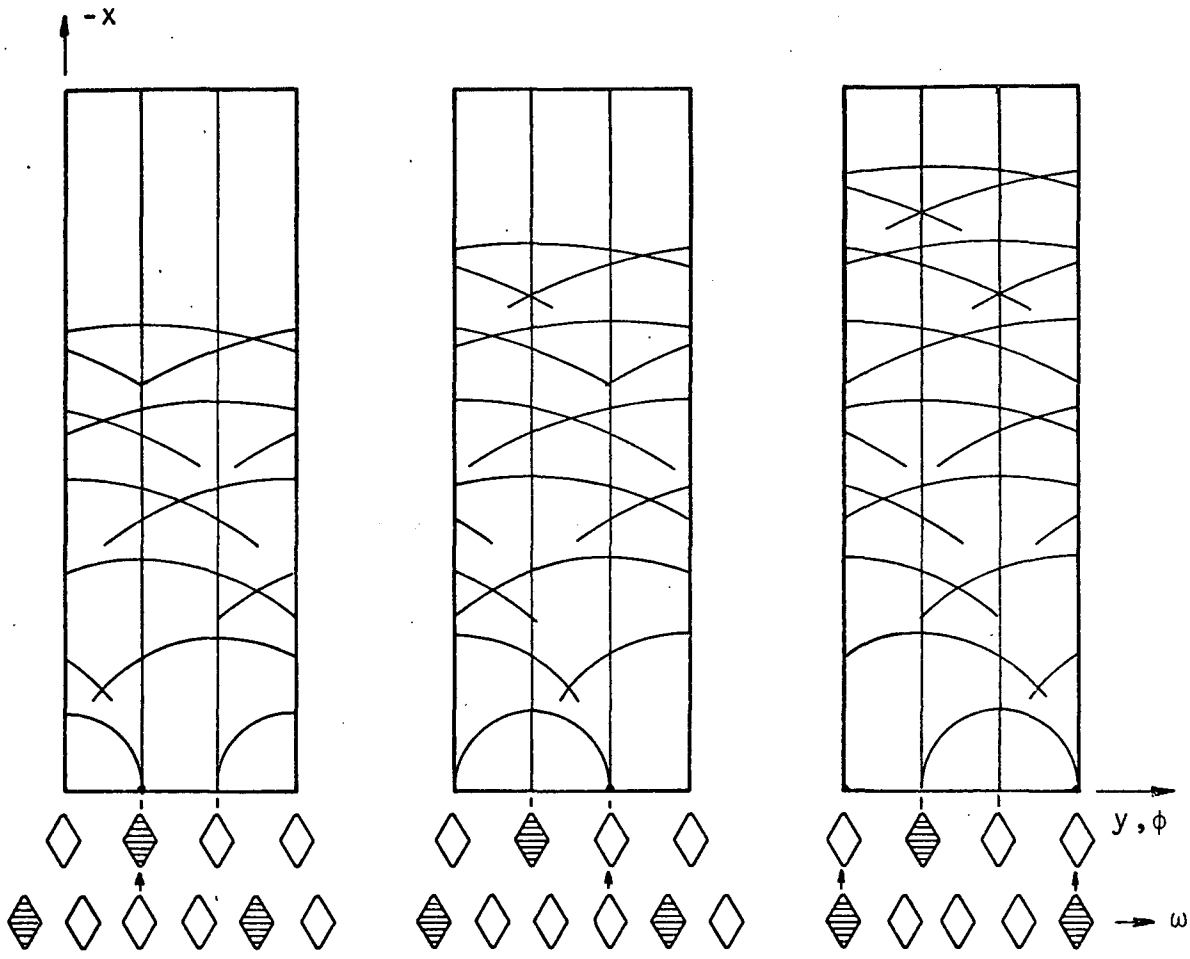

FIGURE 5. (CONTINUED)

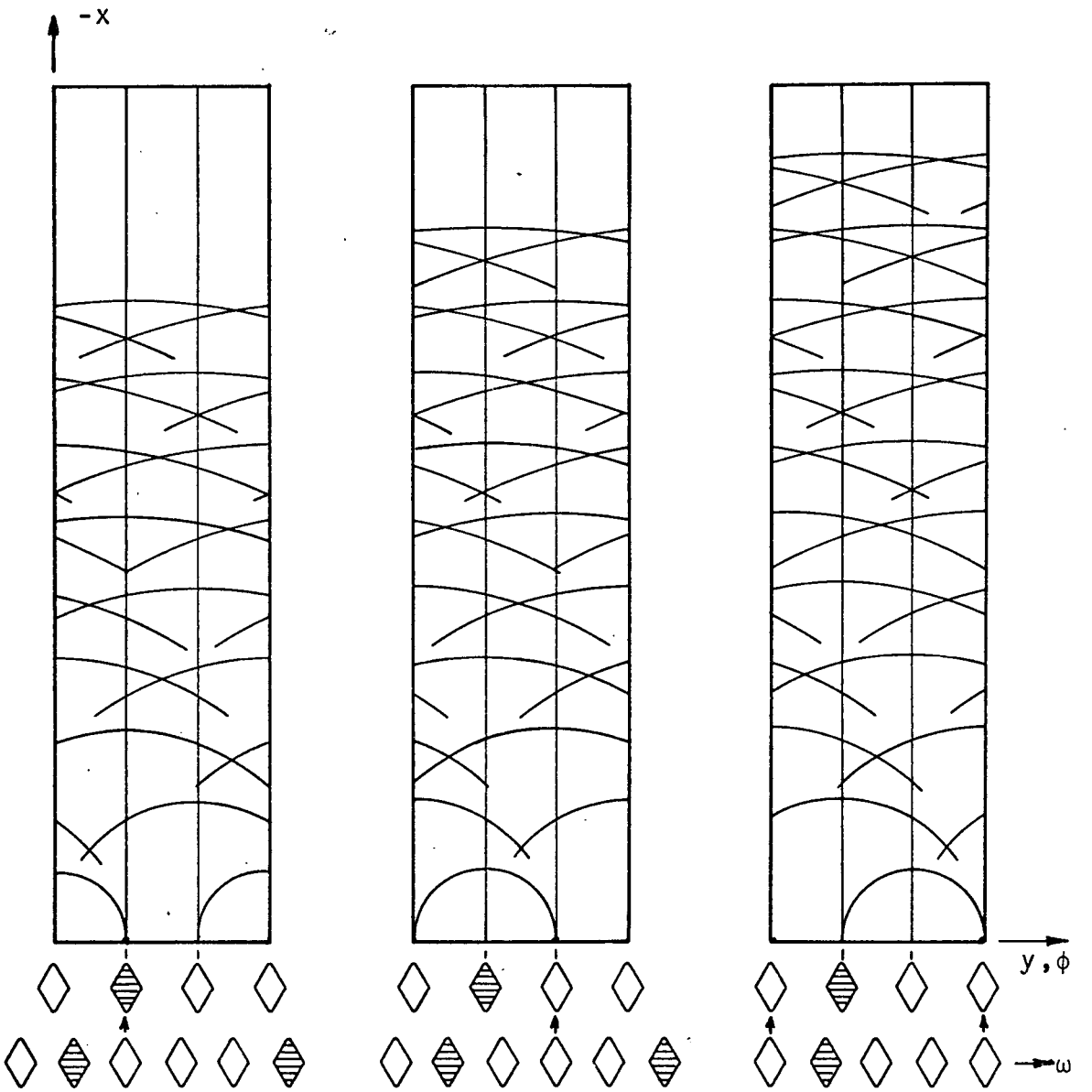

(j) $t = \frac{3}{4} \cdot \frac{2\pi}{\omega}$ $\phi = \frac{3}{4} \cdot 2\pi$

(k) $t = \frac{5}{6} \cdot \frac{2\pi}{\omega}$ $\phi = \frac{5}{6} \cdot 2\pi$

(l) $t = \frac{11}{12} \cdot \frac{2\pi}{\omega}$ $\phi = \frac{11}{12} \cdot 2\pi$

FIGURE 5. (CONTINUED)

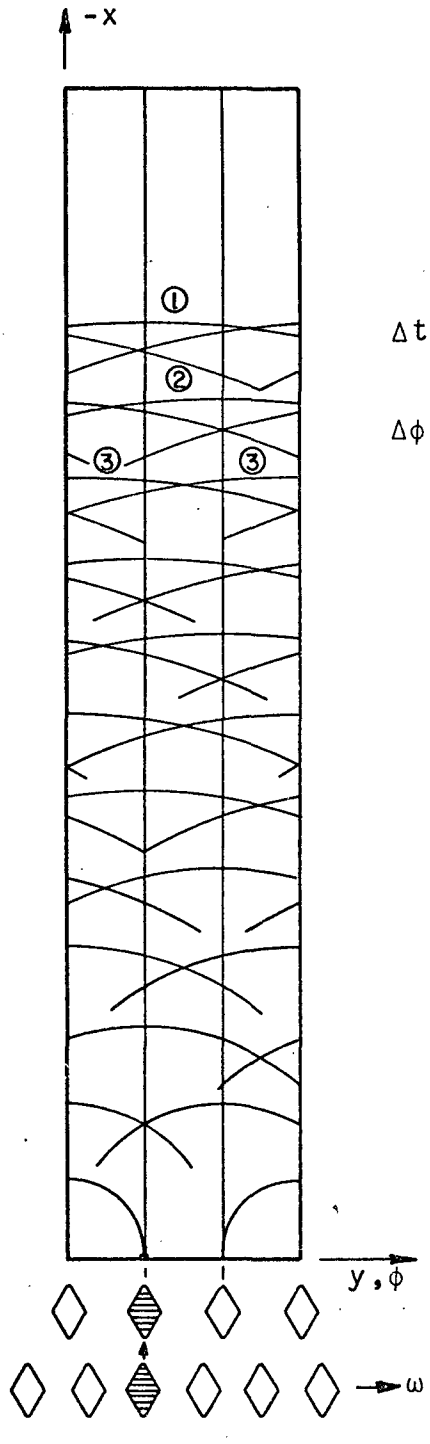

$N = 3$

$M = 4$

$\Delta t = \frac{2\pi}{NM\omega}$

$\Delta\phi = \frac{2\pi}{NM}$

(m) $t = \frac{2\pi}{\omega}$

$\phi = 2\pi$

FIGURE 5. (CONTINUED)

Each time two blades are aligned, indicated by an arrow in Figure (4a) through (4m), a pulse, shown as a large dot at $\chi=0$ above the alignment, is created; this pulse then travels out to form a cylindrical disturbance wave with increasing radius in time. Figure (5a) has a pulse labelled (1) created at t = 0 where the two reference blades (cross hatched) are aligned. This pulse forms the wave, labelled (1) shown in Figure (5b) after $\Delta t = \frac{2\pi}{12\ \omega}$ or $\Delta\phi = \frac{2\pi}{12}$, and a new pulse, labelled (2), is created where the next two blades are aligned (see arrow). These disturbances, (1) and (2), travel out to the positions shown in Figure (5c) and a new pulse, labelled (3), is created where the next set of blades are aligned, (see arrow). The subsequent Figures (5d) through (5m) show the waves travelling out further and new ones being created similarly to Figures (5a) through (5c). The first three waves are identified in Figures (5a) through (5d) and (5m). Figure (5m) can be considered as an asymptotic picture where the wave front in the whole periphery at a distance of $x=(a-u)\cdot 12\Delta t$ is almost flat. If asymptotic configurations at three times are now considered, say at times t_o, $t_o + \Delta t$ and $t_o + 2\Delta t$, as portrayed in Figures (6a) through (6c), several important conclusions can be drawn. Consider first the geometry of the configurations. In Figure (6a) the cross hatched reference or first set of blades are aligned (note the control volume indicated by the dot-dash border, .---., to the top and right of it). In

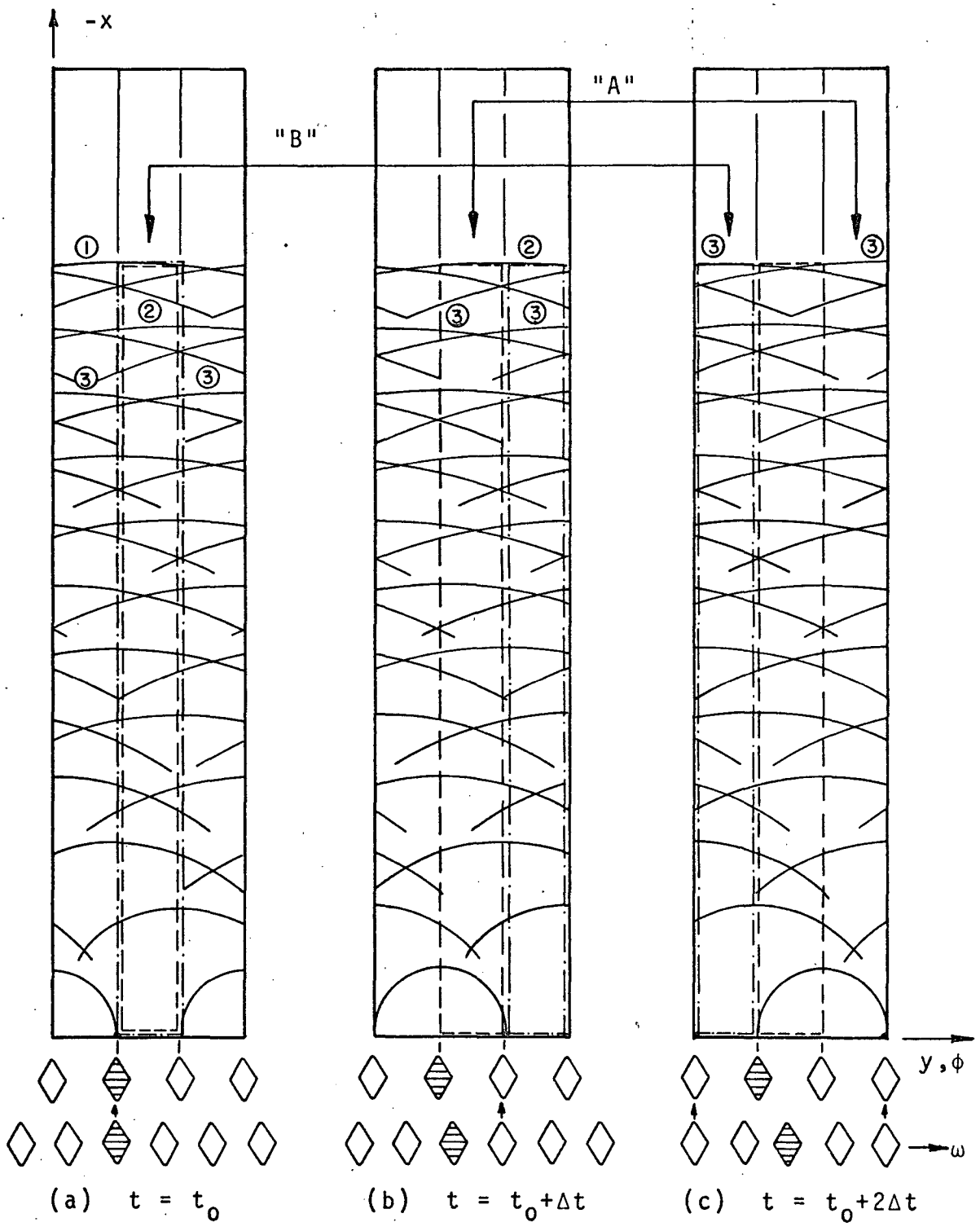

FIGURE 6. ASYMPTOTIC DISTURBANCE PATTERNS GENERATED WHEN A ROTOR BLADE IS ALIGNED WITH A STATOR BLADE.

Figure (6b), representing a time Δt later, the next or second set of blades to the right are aligned (also note the corresponding control volume as described above. Finally, in Figure (6c) $2\Delta t$ after reference time t_o the third set of blades are aligned (this also corresponds to the two blades at the far left of Figure (6c), thus the control volume to the right of this set of blades shall be noted). Each of these dot-dash control volumes correspond to the same relative geometry and it can be seen by direct comparison that the asymptotic wave pattern is identical in each. The same thing is true at all other possible relative blade positions. (this also means all other times)which are encountered as the reference blade of the rotor moves through one complete blade spacing of the stator. It is thus possible to construct the entire asymptotic solution of the periphery at any one instant (and, therefore, at all instances) from all of the asymptotic periodic solutions at successive times found in one blade spacing control volume as the reference blade of the rotor travels through one blade spacing of the stator.

Next consider the dash-dash, ---, control volume always lying to the right of the stator reference blade. This is the reference control volume within which all solutions for the flow upstream of the stator will be found as a function of time. Consider now the asymptotic wave pattern which would be found to the right of the reference control volume at time $t_o+2\Delta t$

in Figure (6c). It is obvious that it is identical to the wave pattern within the reference control value in Figure (6b) at time $t_o + \Delta t$ or one Δt ago (arrows "A"). Next consider the asymptotic wave pattern which would be found to the left of the reference control value at time $t_o + 2\Delta t$ i.e., in Figure (6c). Again it is obvious that it is identical to the wave pattern within the reference control volume in Figure (6a) at time t_o or two Δt ago (arrows "B"). In view of this fact, the appropriate portions of the earlier solutions found in the reference control volume can be applied as boundary conditions to the reference control volume at the current time before proceeding with the computation for the next Δt. This is carried out, refer also to Figure (4a) and (4b), by equating the values at the first row of exterior grid points, say line δ, to the values that existed earlier, Δt ago, at corresponding points, in this case line β, when the geometrical configurations with respect to lines α and β were the same. A similar procedure is carried out for lines α and γ with its own phase lag. In addition, all other horizontal boundaries (those between the blade rows and downstream of the rotor) and vertical boundaries which require phase lags for proper specification are specified analogously. These vertical boundaries are on the downstream side of domain 4 and the upstream side of domain 5.

Consider now the starting process for the computational model.

Figure (7a) through (7m) protrays the computational starting problem comparable to the actual physical one shown in Figure (5a) through (5m). The successive application of the boundary conditions in this manner puts a phase lag into the degree of accuracy of the imposed boundary conditions as the computation is started. As in the actual physical starting process discussed earlier, blade alignment, indicated by an arrow between blades, produces a pulse, indicated by a dot and identified in the first three waves in the Figures (7a) through (7d) and in Figure (7m). Initially there are no previously computed boundary conditions with phase lag to apply, hence, the "tagged" disturbances created in the reference control volume are of minimal accuracy and as such are indicated by using dotted curves. When a more accurate boundary condition is available, i.e., when each side of the reference control volume can be specified from the solution at an earlier time, the accuracy of the solution within the control value will be improved. This is indicated by dashed lines, as for example in Figures (7e) and (7f) etc. The boundary conditions with phase lag are applied as already discussed previously and the arrows in Figures (7a) through (7d) give examples of the phase lag for several cases. As the solution proceeds in time it also becomes more accurate due to the repeated application of increasingly accurate boundary conditions; this is indicated schematically by an increasing solidity of the lines depicting the wave fronts in Figure (7).

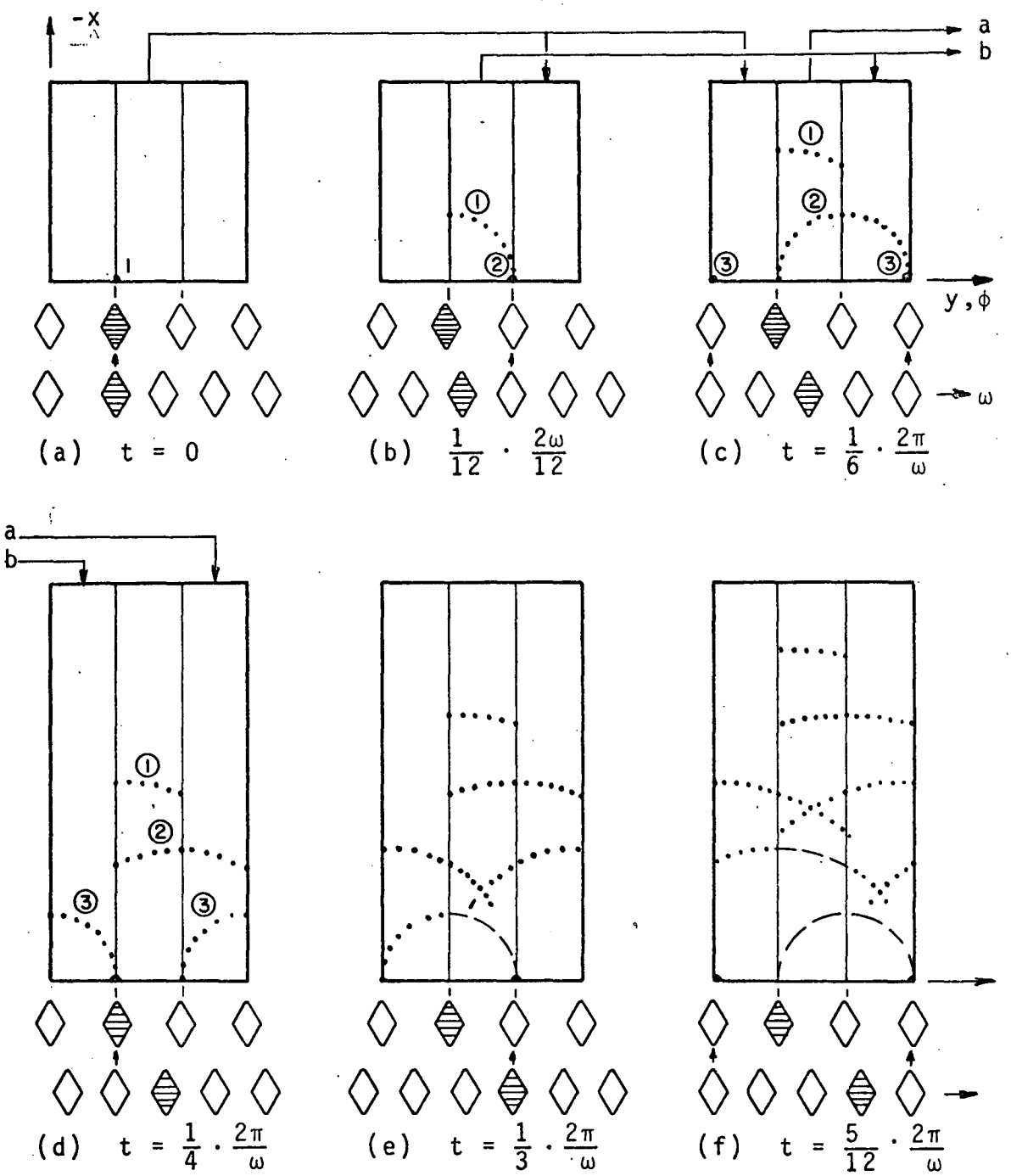

FIGURE 7. STARTING PROCESS SHOWING WAVE DEVELOPMENT OF DISTURBANCE WAVES FORMED WHEN BLADES ARE ALIGNED (SOLUTION WITH BOUNDARY CONDITIONS HAVING PHASE LAG).

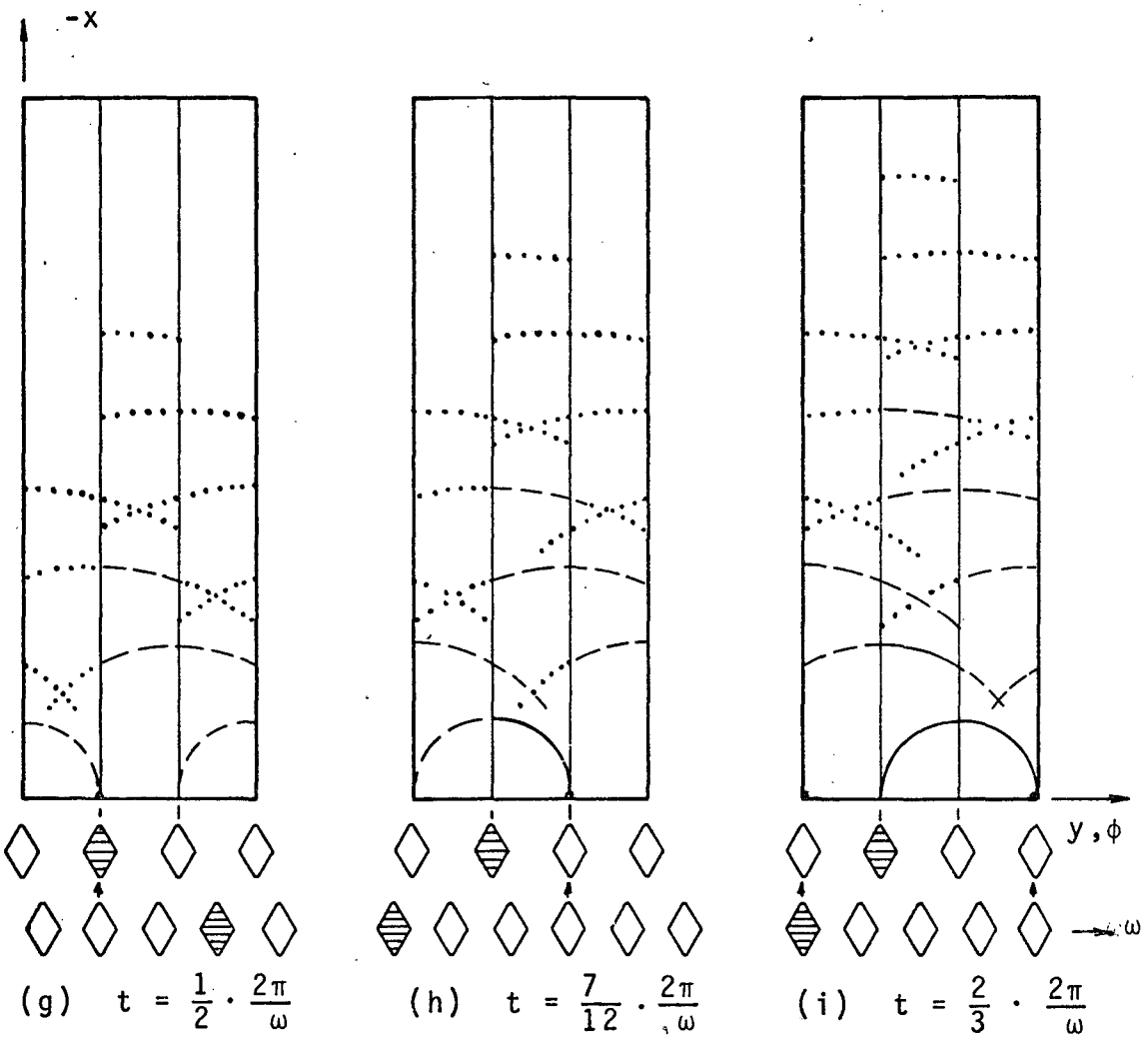

FIGURE 7. (CONTINUED)

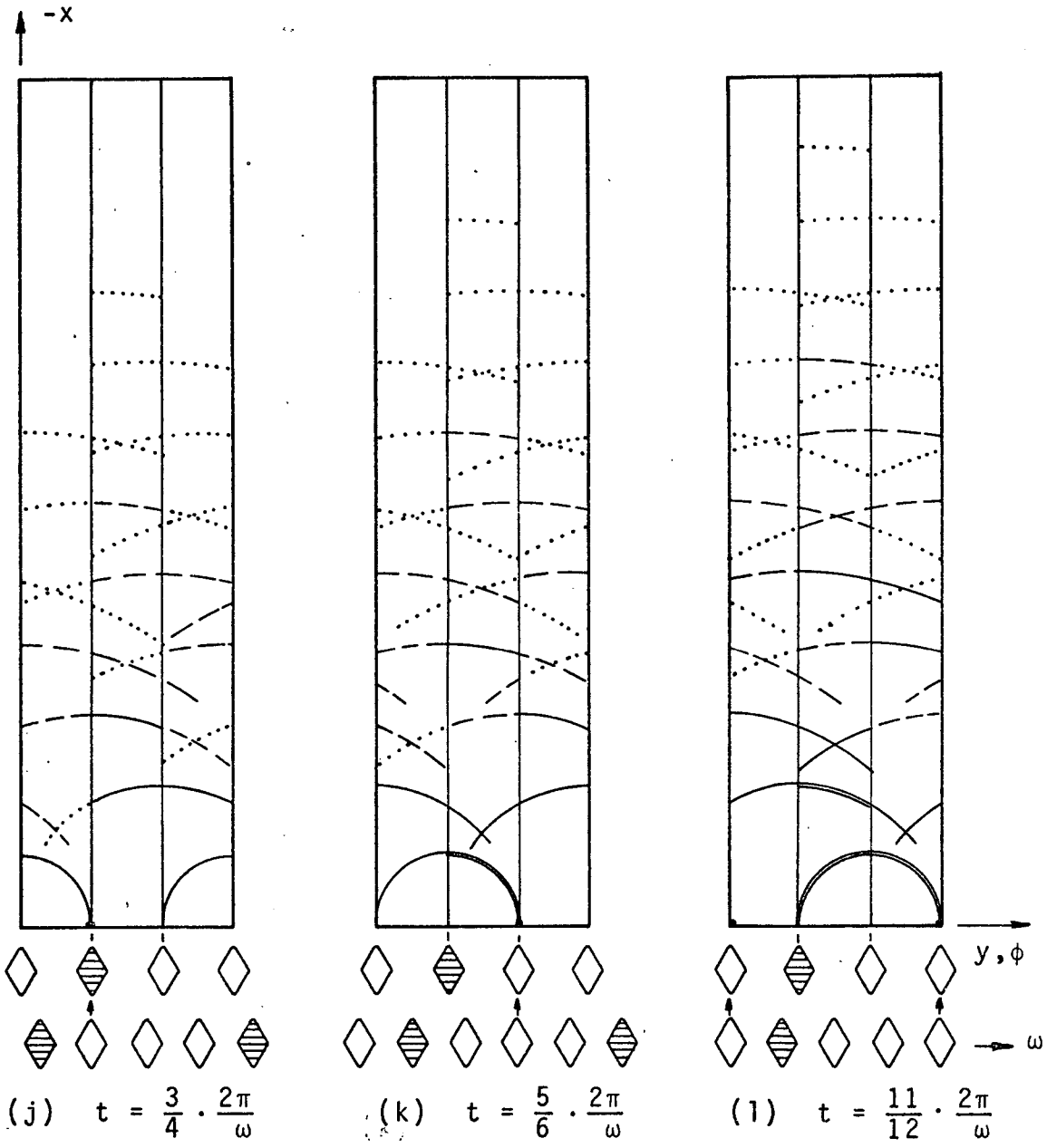

FIGURE 7. (CONTINUED)

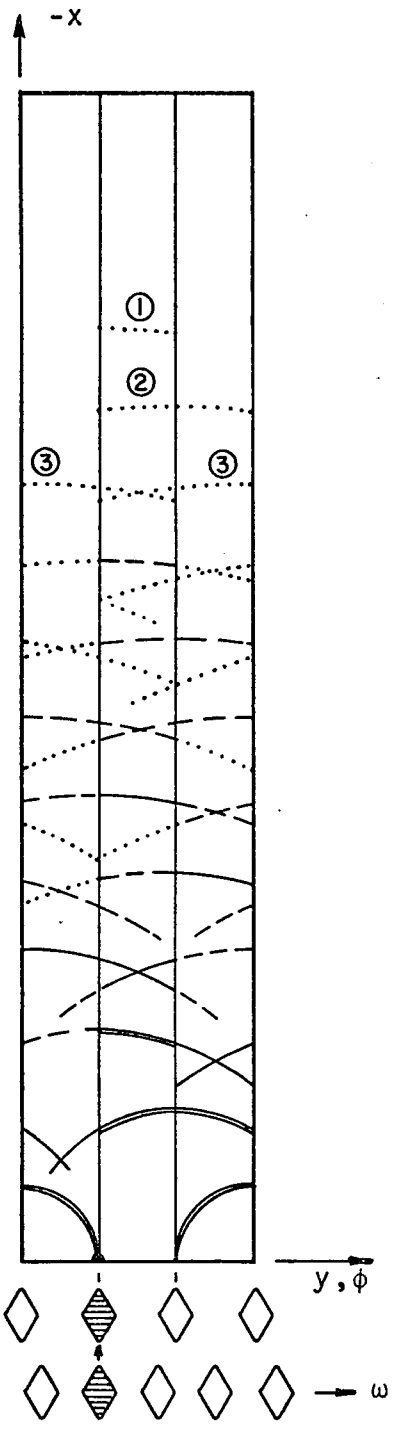

(m) $t = \frac{2\pi}{\omega}$

FIGURE 7. (CONTINUED)

Ultimately all solutions of lesser accuracy propagate and decay at infinity and only the increasingly more accurate disturbances remain. The result is that the waves associated with the approximated starting process are lost and the solution becomes asymptotic the same as shown in Figures (6a) through (6c). The criterion which determines the improvement is not the anguler distance that the rotor has travelled, but is the number of times the boundary conditions have been applied; consequently, the larger the number of blades, the better is the solution after a complete revolution of 2π. An asymptotic periodic solution exists when successive solutions possess periodic relationships and phase lags with respect to each other so that these periodic relationships and phase lags correspond precisely to those imposed by the method of boundary condition application.

Horizontal Surfaces The horizontal surfaces are specified by the previously discussed technique which is based on the fact that these surfaces are "planes of equivalence" with a phase lag. Figure (8) shows a typical domain. A row of "virtual" grid points in this case k = 1 and K = KSP is placed one mesh point outside the calculation domain at which the flow conditions are equal to those existing at corresponding grid points one mesh point inside the opposite boundary, in this case K = KSM and K = 3 respectively, at a time when the blade positions at that opposite boundary were the same as currently exist

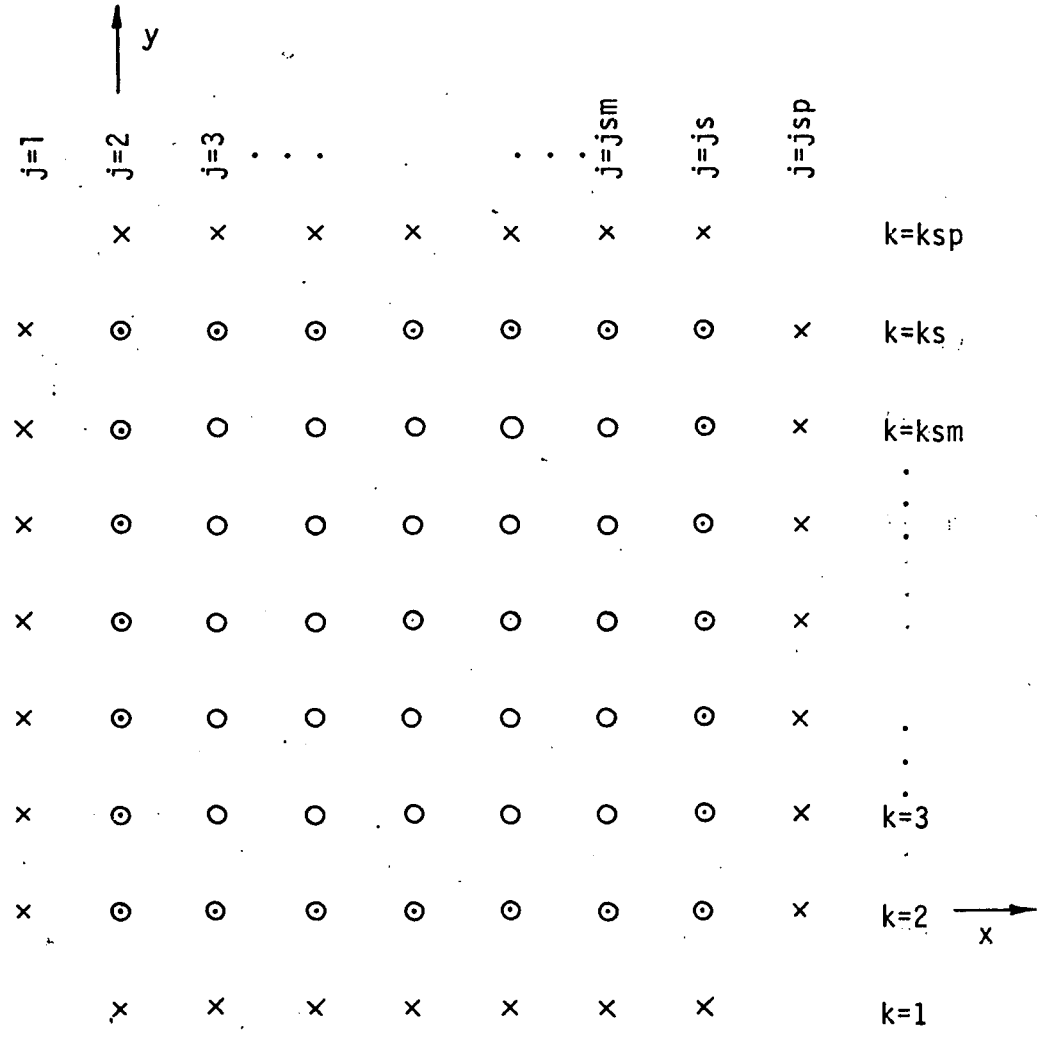

FIGURE 8. SCHEMATIC OF A TYPICAL TRANSFORMED SQUARE DOMAIN

along the subject boundary.

Specifically the phase lags for these horizontal boundaries are as follows: Let there be N blades in the upstream blade row and M blades in the downstream blade row with $N \leq M < 2N$. Also let n be the number of time steps required for one blade spacing of the larger gap to be traversed and m the number of time steps required for the smaller gap to be traversed. There results first of all

$$Nn = Mm \tag{17}$$

There are four sets of boundaries to be considered. These are and consist of:

A. The upper left set consisting of domains 1,2 and 4, adjacent to K=KS.

B. The upper right set consisting of domains 6 and 7, adjacent to K=KS.

C. The lower left set consisting of domains 1,2 and 5, adjacent to K=2.

D. The lower right set consisting of domains 6 and 7, adjacent to K=2.

The specific phase shifts are as follows:

(1) A at K+KSP = C at K=3 (n-m) time step ago

(2) B at K+KSP = D at K=3 (n-m) time step ago

(3) C at K=1 = A at K=KSM (m-(n-m)) time step ago

(4) D at K=1 = B at K=KSM (m) time step ago

The values computed at every time step at K=3 and KSM must, thus, be stored for later use. Since a considerable number of time steps are involved, this cannot be done using the program core and is done instead by disk or tape storage and recall.

Inflow and Outflow Boundaries The transformation for x in domains 1 and 7 remove the extreme boundaries (for J=2) 1L and 7R (for J=JS) to $\pm\infty$ at which point the disturbances will have decayed so that steady compressor performance values can be assigned there. Virtual grid point values for all other vertical surfaces, except 3R, 4L, 5R and 6L, when displacement thickness on the blades are included, are determined from the computed values located within the adjacent domain so that spatially they are in the same position. Refer to Table I for this and the following discussion for specific distribution of equivalents. Virtual grid point values for 3R and 5R are evaluated by reworking the inflow from 4L and 6L into step profiles (to account for displacement thickness) and for 4L and 6L by reworking the outflow profiles from 3R and 5R respectively from step-like profiles (due to displacement thickness) into wake-like

TABLE I

EQUIVLANETS WITH AND WITHOUT PHASE LAG

Domain and J (Exterior)		Domain and J (Interior)	Comments
1 (2)	=	$-\infty$	Free stream
1 (JS)	=	2(2)	
2 (1)	=	Interpolated between 1(JSM) and 1(JS)	
2 (JS)	=	3(2)	
3 (1)	=	2(JSM)	
3 (JSP)	=	4(3)	Reworked when δ^* is included.
4 (2)	=	3(JS)	Reworked when δ^* is included.
4 (JS)	=	5(2)	Interpolated with or without phase lag.
5 (1)	=	4(JV)*	Interpolated with or without phase lag.
5 (JSP)	=	6(3)	Reworked when δ^* is included.
6 (2)	=	5(JS)	Reworked when δ^* is included.
6 (JSP)	=	Interpolated between 7 (2) and 7 (3)	
7 (2)	=	6(JS)	
7 (JS)	=	$+\infty$	Downstream

*JV determines C4 (see Figure 1a), C4 = C2/(JS-JV).

profiles. It is to be noted that in order to obtain spatially equivalent grid points for boundaries 4R and 5L account has to be taken of the relative motion of the blades and interpolation of quantities as well as phase shifts are required.

In the case of equal blade spacing for adjacent stages matching flow variables along surfaces 4R and 5L is straightforward; in any other case certain subleties accrue in the process of minimizing the computer storage and time requirements. Again a column of grid points external to domains 4 and 5 are considered. In the regions of overlap shown in Figures (9a) and (9b), it is clear that the exterior column of points from domain 4 overlaps the interior of domain 5, and vice versa. However, for the regions of "non-overlap" determination of the flow variables at these exterior grid points is accomplished by a phase lag technique, analogous to the equivalence technique discussed above, which is based on the blade positions during a full cycle of movement of domain 5 relative to domain 4. In the case of equal spacing the time-delay is zero, and the regions of non-overlap labelled "left" and "right" in Figure (9a) have a direct correspondence. On the other hand, in the case of fractional (non-integer) spacing the matching of conditions along the region non-overlap must be based on a correspondence of relative

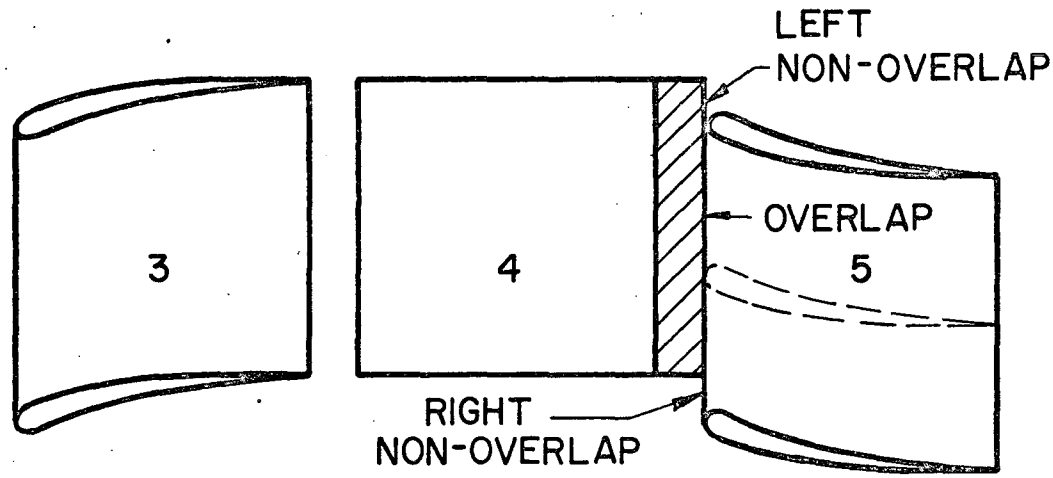

(a) Integer Multiple Domains (—1:1, ---2:1)

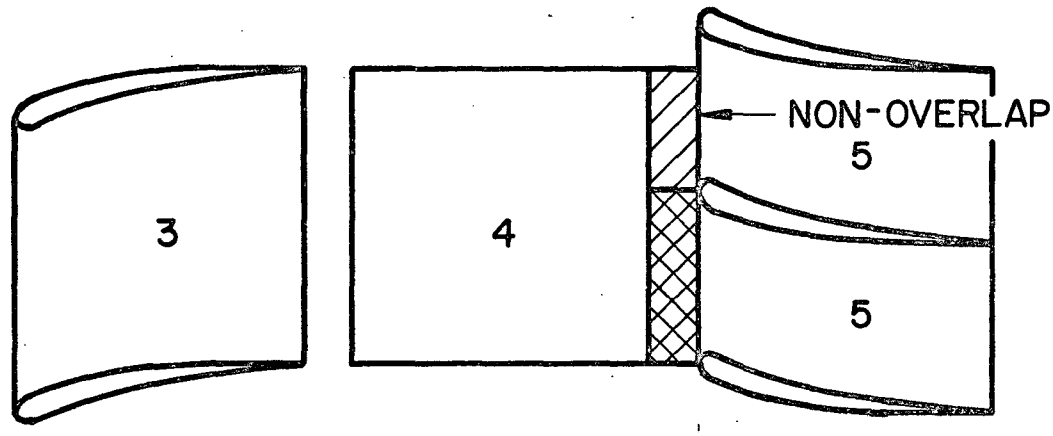

(b) Fractional Multiple Domains ($1:1 \leq M/N < 2:1$)

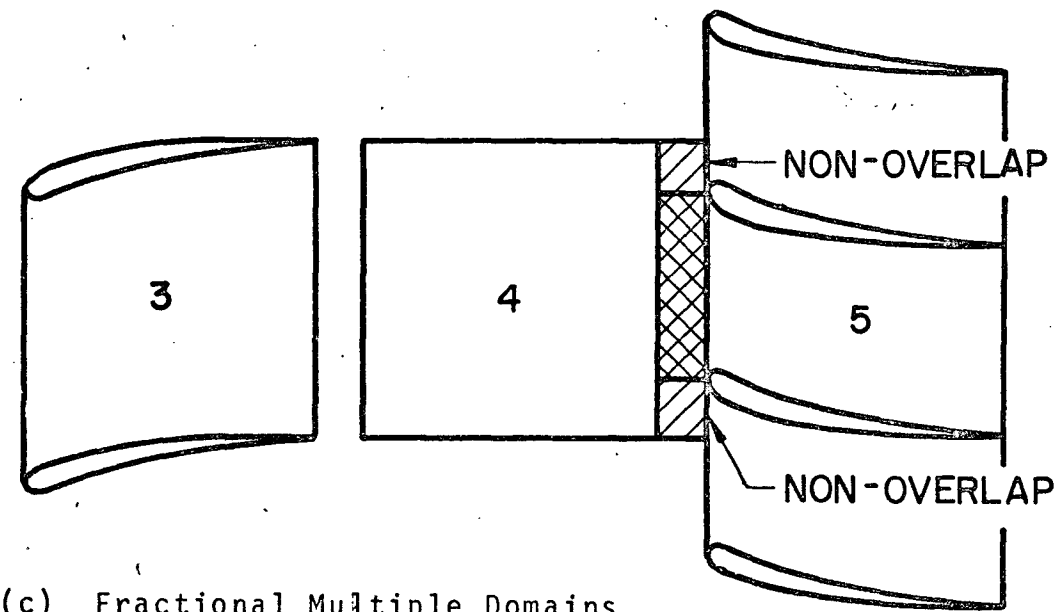

(c) Fractional Multiple Domains
(at Later Time)

FIGURE 9. VERTICAL BOUNDARIES BETWEEN DOMAINS 4 AND 5.

blade positions, which introduces a phase lag in the boundary conditon applied on surface 4R and 5L.

This phase lag is analogous to that discussed earlier for the horizontal boundaries. The only added feature is that up to three separate sets of data each with its appropriate phase shift must be applied since the overlap can be such as shown in Figure (9c) which clearly shows three regions where data must be provided. Thus the J = JS values for domain 4, refer to Figure (8), are equal to the J = 2 values of domain 5 at phase shift times having up to three different values, as discussed earlier, and the J = 1 values for domain 5 are equal to the J = JSM values for domain 4 at phase shift times having up to two different values. Even though only two are needed, three are specified since the non-overlap region can be either above or below the larger blade gap. The interpolation merely ignores the extra values.

The upstream infinity boundary is completely specified by imposing the pressure, p, temperature, T, the axial velocity, u and the normal velocity, v. This determines the value of the incoming mass flow, momentum flux and total enthalpy flux. The time-averaged outgoing mass flux when integrated over the complete peripheral annulus of the compressor is necessarily equal

to the incoming value when the compressor operating conditions are fixed Since the upstream and downstream infinity boundaries are assumed to have steady flow, the product of density and axial velocity at the downstream boundary is taken to be equal to that at the upstream boundary

$$\rho_e u_e = \rho_\infty u_\infty \tag{18}$$

The total enthalpy flux at the downstream boundaries will differ from the inflow value by the work done by the compressor on the fluid. This difference is evaluated by determining a time and space averaged normal velocity component, v_i, at some station between the two blade rows and determining the relative total enthalpy of the downstream stage with respect to the relative total enthalpy of the upstream stage:

$$H_{R1} = H_{R2} + (v_i+\omega_1 r)(\omega_1 r-\omega_2 r) \tag{19}$$

where ω_1 and ω_2 are the angular velocities of the two respective stages and r is the mean radius of the blades. Since the relative total enthalpy is constant

$$H_e = H_{R2} \tag{20}$$

The normal component of velocity at the exit, v_e, is determined by use of the normal momentum equation

$$\rho_e u_e v_e = \rho_i u_i v_i + \int p_n dx \tag{21}$$

where $p_n dx$ is the time averaged normal component of pressure integrated over the horizontal projection of the upper and lower blades of the downstream stage. The axial momentum equation

$$\rho_e u_e^2 + p_e = \rho_\infty v_\infty^2 + p_\infty - \frac{\left\{(DRAG1 - \int p_n dy) - (DRAG2 - \int p_n dy)\right\}}{\int_{y_e}^{y_u} dy} \quad (22)$$

(Where DRAG1 and DRAG2 are the boundary layer drag contributions discussed earlier and $\int p_n dy$ is the horizontal component of pressure along upper and lower blade surfaces) provides the variable $\rho_e u_e^2 + p_e$. Thus the flow variables $(\rho_e u_e)$, $(\rho_e u_e^2 + p_e)$, v_e and H_e are inserted into the definition of total enthalpy.

$$H_e = \frac{\gamma}{\gamma-1}\frac{p_e}{\rho_e} + \tfrac{1}{2}(u_e^2 + v_e^2 - \omega_2^2 r^2) \quad (23)$$

to solve for the pressure p_e and subsequently

$$u_e = \frac{(\rho_e u_e^2 + p_e) - p_e}{\rho_e u_e} \quad (24)$$

and

$$\rho_e = \frac{\rho_e u_e}{u_e} \quad (25)$$

Thus the downstream boundary conditons are completely specified in terms of the upstream boundary conditions and the compressor work.

The application of the boundary conditions, as described above, will asymptotically impose periodicity at the boundaries; the non-steady computation within the calculation domains will, therefore, yield asymptotically a periodic solution. The solution will automatically contain the stationary and travelling waves as well as the nonuniform flow at the trailing edge of the balde rows due to boundary layer and/or wake formation.

It is emphasized that the development of this technique does not assume axial symmetry or existence of a peripherally periodic solution having wave length less that 2π. It is only assumed that the flow very far upstream of the fan or compressor is uniform. The peripheral distortion that results at the fan or compressor face due to the interaction of an unequal number of blades in the rotor and stator is obtained by considering a single blade-to-blade passage as a function of time with the appropriate phase lag in the imposition of boundary conditions on the peripheral (horizontal) boundaries. The peripherally distorted flow field pertaining to the entire annulus, consisting of all blade-to-blade passages, at any instant can then be deduced from the non-steady solution for the single passage after periodicity (in time) has been attained.

The time requirement to establish periodicity in the most general case is, in principle, one complete wheel revolution however, a fraction of a revolution is probably sufficient in most practical cases since the strength of the disturbances emitted decays rapidly with distance from the fan or compressor. The strongest disturbances are the shock waves emitted by a supersonic fan or rotor, which will decay linearly with distance[11], in the absence of interference effects. The decay rate for a wave train will be faster due to destructive interference between a trailing wave and the leading wave of the next disturbance. Consequently the time to reach a periodic solution will be less than a complete wheel revolution; the numerical results obtained thus far suggest it will be a small fraction of a revolution.

D. Boundary layer analysis. One of the principal phenomena contributing to the non-steady flow components in compressors is the passage of a downstream blade through the wake of an upstream blade. The development of the boundary layer and wake must thus be included in any study which proposes to give a meaningful representation of the non-steady disturbances (including noise) in the flow field around and through a compressor. After due consideration, it has been concluded that a detailed analysis of the boundary layer itself is inappropriate in the present context. It is the wake shed by the blades which is of immediate concern, and the wake

carries only integral type information about the upstream boundary layer, e.g., total skin friction drag as opposed to local skin friction coefficient. Certain simplifications and assumptions are, therefore, invoked based on the von Karmen integral relations. Thus the displacement thickness and shape factor are the quantities which are determined along the blades so that the displacement effect and momentum loss due to skin friction can be evaluated. This is necessary not only for correctly evaluating the flow between blades but also specifying the downstream boundary for a given set of upstream conditions. The choice of laminar or turbulent viscosity coefficients is determined by the local Reynolds number, $R_e = \rho ux/\mu$ and its comparison to a crictical Reynolds number.

The boundary layer is treated as quasi-steady; that is, at any given instant of time the boundary layer is assumed to be a function of space variables, in this case x, only. In other words the time required for the boundary layer to adjust itself is assumed to be much less than the time required for changes to take place in the flow field. This permits the equating of the partial and total derivatives with respect to x and allows for a reduction in the complexity of the boundary layer representation.

(a) Displacement Thickness - The displacement thickness, δ^*, at any point is formed by evaluating

$$\frac{d\delta^*}{dx} = A(R_e)^{-B}$$

and forming

$$\delta^*_{i+1} = \frac{d\delta^*}{dx} (\Delta x) + \delta^*_i$$

where (a) and (b) are coefficients which depend on the state of the flow. (b) is 0.5 for laminar flow and 0.2 for turbulent flow. (a) is a parameter determined as follows. Solutions of the Falkner-Skan equation for laminar flow give

$$A = \tfrac{1}{2} \left(\frac{2}{m+1}\right)^{\frac{1}{2}} h(\beta)$$

with

$$\beta = \frac{2m}{M=1}$$

and

$$m = \frac{x}{u} \frac{du}{dx}$$

where $h(\beta) = \eta - f$

is a curve fit of the Falkner-Skan solutions (Reference 12). For turbulent flow a velocity profile

$$\frac{u}{U} = \left(\frac{y}{\delta}\right)^{(1/n)} \tag{32}$$

is assumed with n an input to the program and

$$A = \frac{0.8}{(n'+1)} \left[\frac{0.027(1+n')\ (2+n')}{n} \right]^{0.8} \tag{33}$$

where

$$n' = n - \frac{kp_x}{\{1 + (kp_x)^2\}^{\frac{1}{2}}} \tag{34}$$

$$p_x = \frac{dp}{dx} \tag{35}$$

and k is an input to the program. Thus n' differs from n by at most 1. This representation of the turbulent power law profile could be further modified if necessary by multiplying the second term on the right hand side by Equation (33) by another constant, say k'; then k' would determine change of n' from n.

(b) Drag or Momentum Loss - the drag due to the boundary layer at the surface of the blades is found by evaluating the local shear stress (Reference 13).

$$\tau = \frac{U^2}{H} \left(\frac{d\delta^*}{dx}\right) - \delta^* \left[\frac{(2-M^2)}{H} + 1\right] \frac{dp}{dx} \tag{36}$$

and integrating it numerically along the surface to give the drag of one side of the blade, namely

$$\text{DRAG} = \sum_i (\tau_i dx_i) = (\Sigma \tau_i)\, dx \tag{37}$$

the shape factor H is determined for laminar flow from

$$H = \frac{\delta^*}{\theta} = \frac{\int_0^1 (1-f')d\eta}{\int_0^1 f'(1-f')\, d\eta} = \frac{n - f}{f - \int_0^1 (f')\, d\eta} \tag{38}$$

and

$$g(\beta) = f - \int_0^1 (f')^2\, d\eta \tag{39}$$

so that $g(\beta)$ (Reference 12), as well as $h(\beta)$, is a curve fit. for turbulent flow

$$H = \frac{(2+n')}{n'} \tag{40}$$

(see Reference 14). M in Equation (36) is the Mach number. Total drag of a blade is the sum of the lower and upper surface contributions. This total drag is then deducted from the momentum of the inviscid flow contained between the trailing

edges of the blade pair in question.

A blade wake having a thickness approximately equal to that of the boundary layer at the trailing edge, but not less than the finite difference grid size, is then included in the inviscid flow at the trailing edge. This wake is formed such that the total fluxes of mass, momentum (including now the skin friction drag) and energy are conserved at the trailing edge of each blade row.

Therefore, the blades of the following blade row will move through a flow field which includes the wake of the upstream blade row as represented by thin regions having correct integrals of mass and momentum defect and approximately correct thickness. The development of the boundary layers on the downstream blades will be calculated in the manner described above, and by the same procedure will also form wakes which will persist in the downstream direction.

III. DEMONSTRATION OF THE METHOD

A. Verification of the numerical solution. Application of the computer program under development to analysis of the configuration shown in Figure (10), consisting of an infinite cascade of non-rotating symmetric airfoils, was carried out as a verification test of the numerical method. Of particular concern was the ability of the numerics to provide a reasonably accurate rendition of the leading edge singularity.

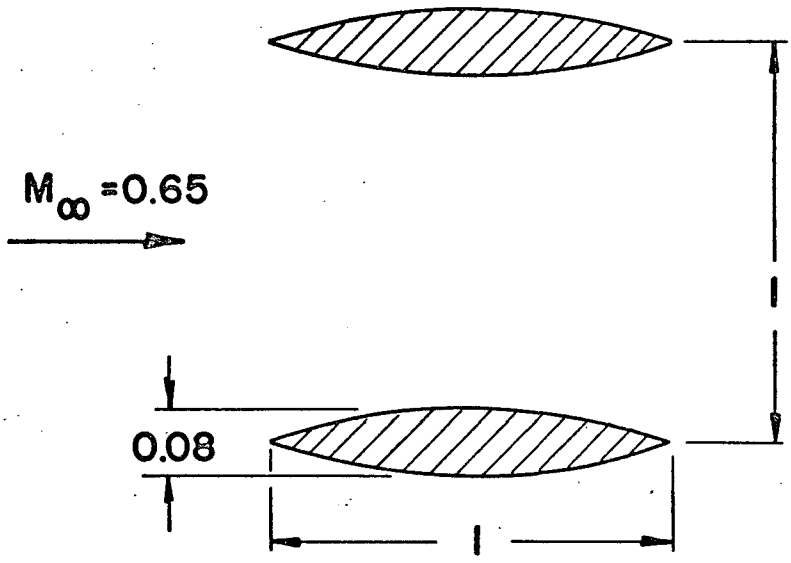

FIGURE 10. TEST CONFIGURATION

Figures (11) and (12) show the Mach number and pressure distributions, respectively, obtained over the airfoil surfaces. Figure (11) also shows a comparison of the present results and those

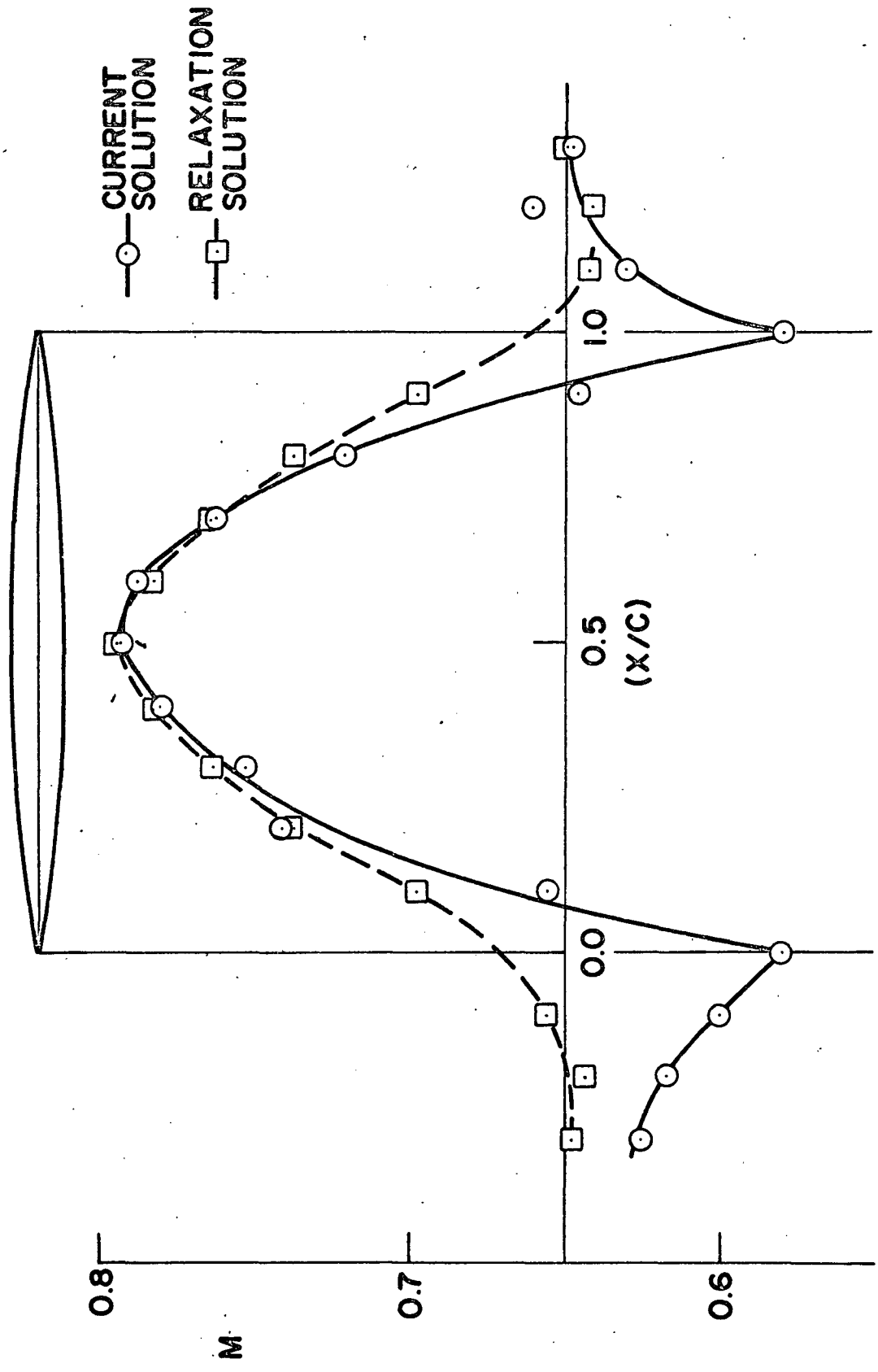

FIGURE 11. MACH NUMBER DISTRIBUTION OVER SYMMETRIC AIRFOIL IN INFINITE CASCADE

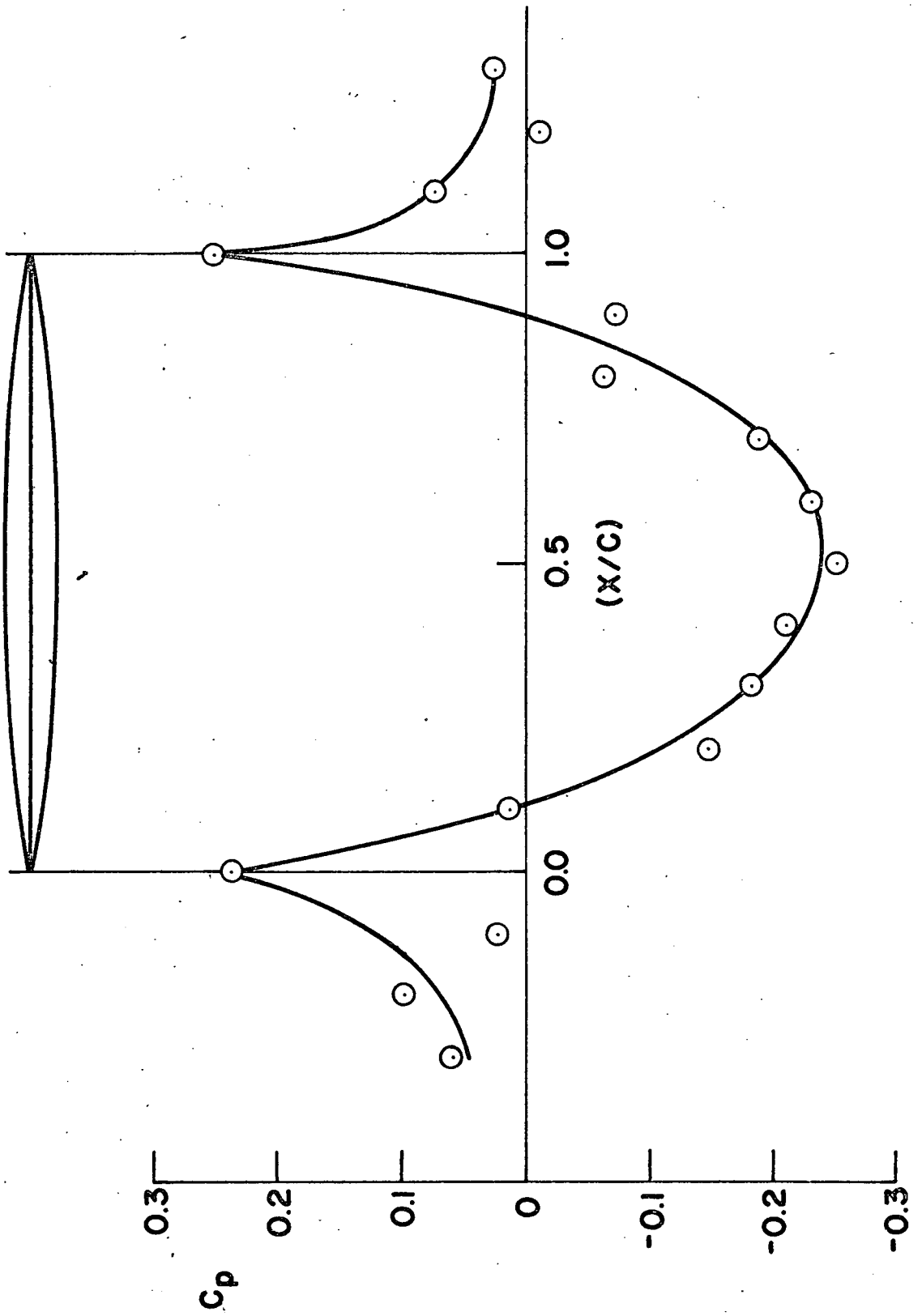

FIGURE 12. PRESSURE DISTRIBUTION OVER SYMMETRIC AIRFOIL IN INFINITE CASCADE

computed by the relaxation technique of Katsanis[15], using the same grid spacing. Excellent agreement is found over the central part of the airfoil and it appears that the present results are reasonably accurate near the singular points, even with an admittedly coarse grid (Δx = 1/10 chord).

B. Illustration of rotor-stator interaction. A rotor-stator configuration which incorporates thickness, camber and angle of attack effects, pictured in Figure (10), was selected to illustrate the ability of the method to analyze non-steady flows due to interaction of adjacent blade rows. The upstream stationary blades are again 8% thick but cambered such that the upper surface is a straight line inclined at -45^{o}. The downstream rotating blades are the same 8% thick uncambered symmetric airfoils as previously studied but with the mean line inclined at $+45^{o}$. The solidity is unity. The free stream velocity vector is alinged at -45^{o} and the Mach number is 0.65. The rotational speed of the rotor is $\sqrt{2}$ times the free stream velocity. Thus, if the blades has neither thickness or camber they would produce no flow deflection or work. This general configuration was initially selected to correspond to that considered by Kemp and Sears[7], however, the Mach number and blade thickness were selected to correspond to the previous calculation of an isolated blade row. Consequently, significant compressibility effects were introduced which precluded a direct comparison with the Kemp and Sears solution.

This stator-rotor configuration produced, after 480 time steps, the instantaneous surface Mach number distribution shown in the lower portion of Figure (13). An imbedded supersonic region is clearly evident. The corresponding pressure distribution is shown in Figure (14). This figure, in addition, shows the pressure distribution on the line midway between the blades (indicated as mean). Results for long times indicate practically the same distribution, altered slightly by the blade interaction phenomenon.

The pressure variation at the two points labelled (6,7,2) and (6,7,7) downstream of the rotor, see Figure (13), is shown in Figure (15).* These variations, discounting the initial starting transient, have a frequency of about 1 cycle per 80 time steps, which corresponds to the natural frequency of the rotating system, i.e., 80 time steps is the blade passing frequency. This same frequency manifests itself in the peripheral (Y) and axial (X) force variation on the rotating airfoils as shown in Figure (16).

The corresponding pressure variation at points (2,7,2) and (2,7,7) upstream of the stator are shown in Figure (17). These varia-

*These points are in a coordinate system rotating with the stator. Thus the noted time variations are directly attributable to the rotor-stator interactions rather than quasi-steady variations associated with the rotor blade passing a fixed point in space. Obviously, the results at a fixed point can also be obtained from the solution and will be discussed later.

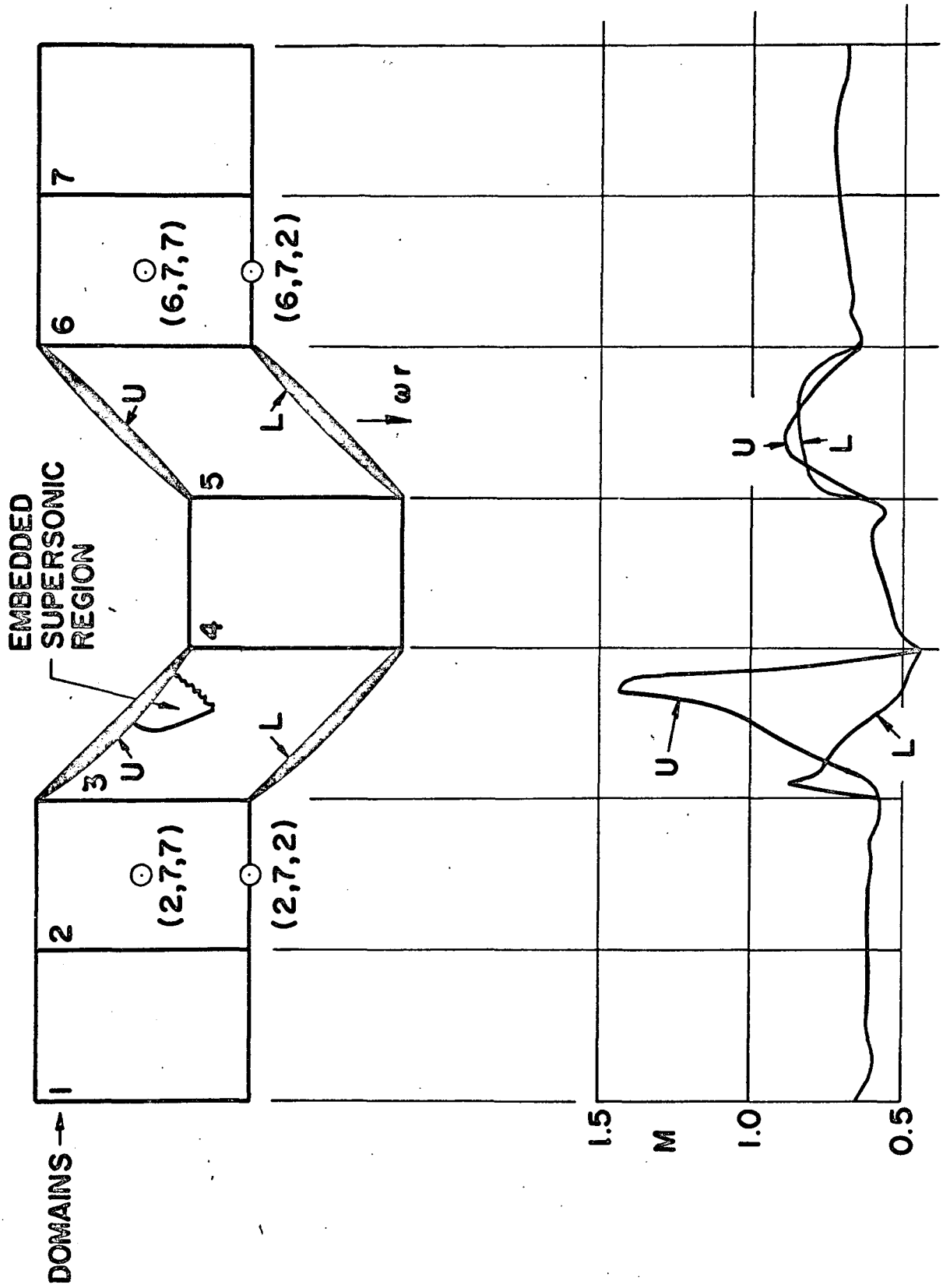

FIGURE 13 . IDENTIFICATION OF GEOMETRY AND MACH NUMBER DISTRIBUTION

C: 2

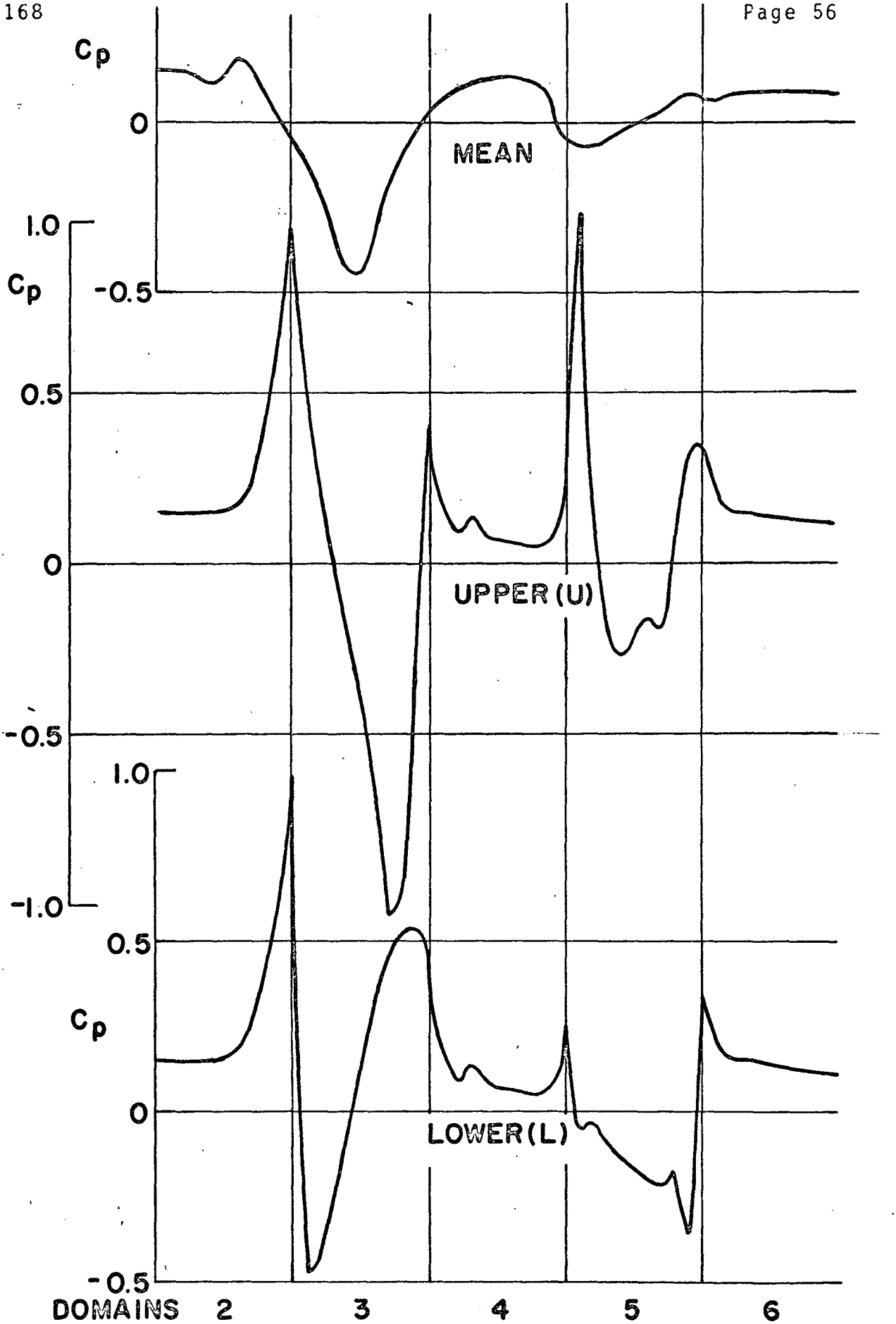

FIGURE 14. PRESSURE DISTRIBUTIONS ALONG UPPER(U) AND LOWER(L) BOUNDARIES AND MEAN LINE

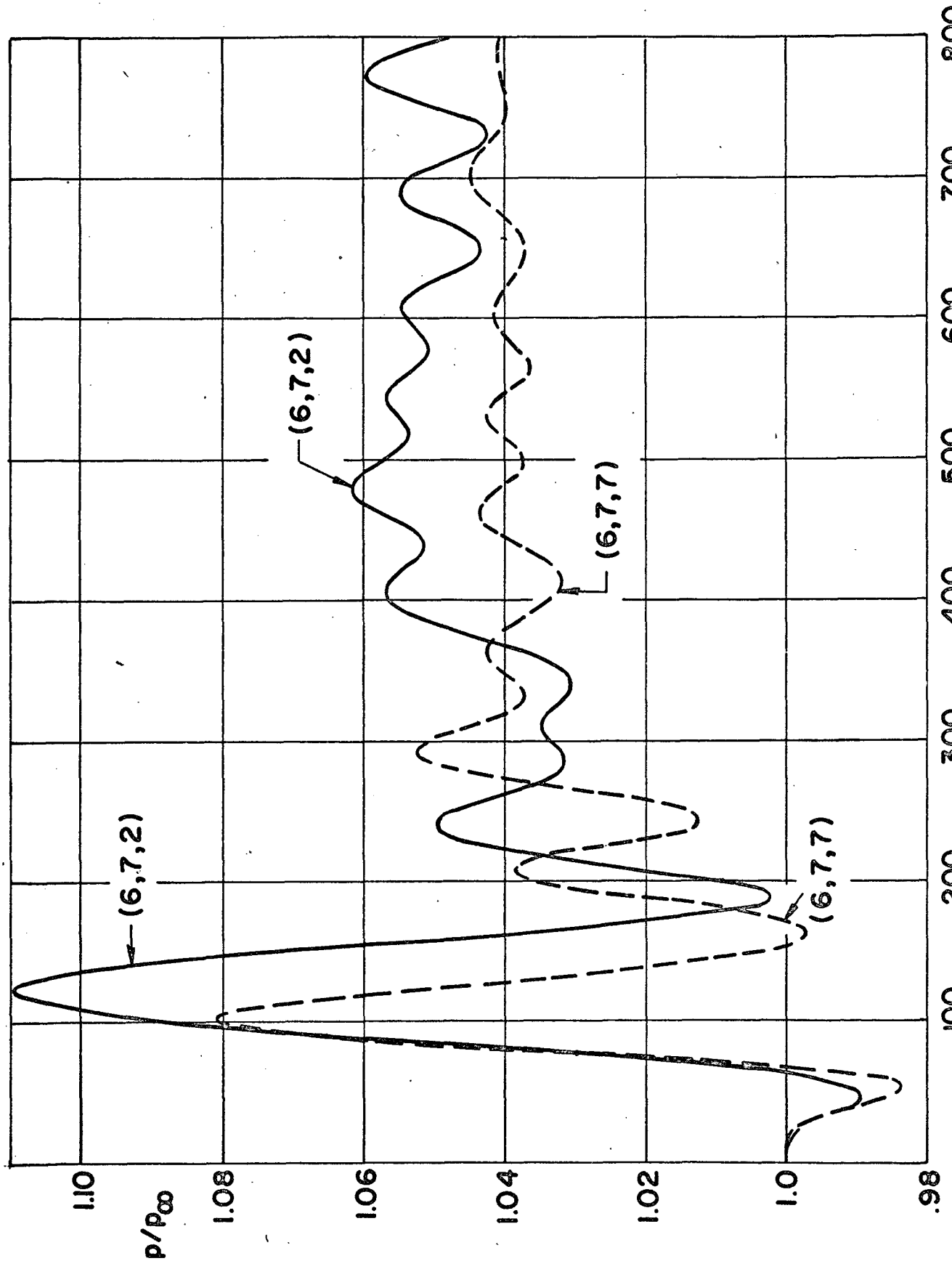

FIGURE 15. PRESSURE VARIATION AT POINTS (6,7,2) AND (6,7,7) DOWNSTREAM

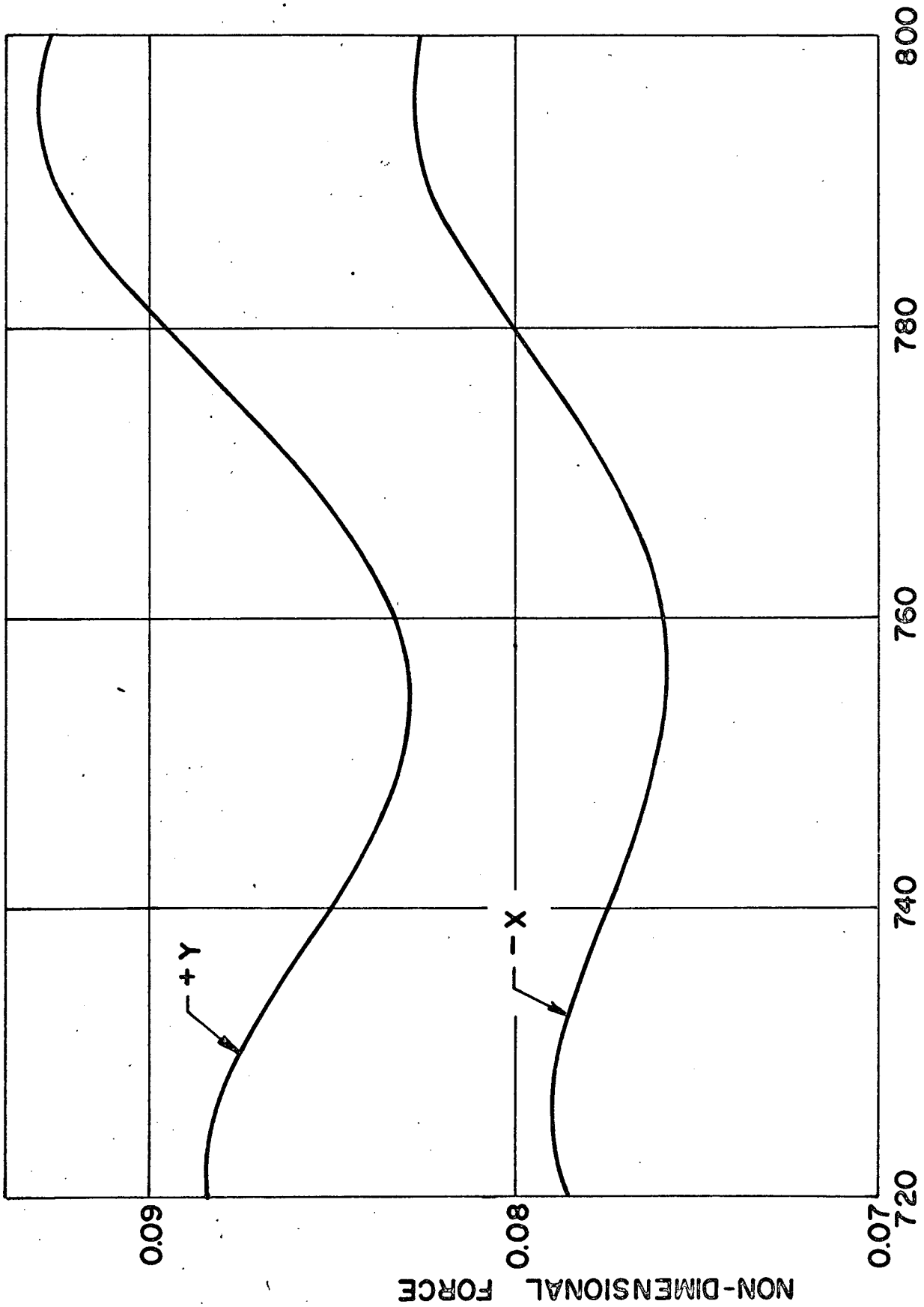

FIGURE 16. PERIPHERAL (Y) AND AXIAL (X) FORCE ON ROTATING BLADES

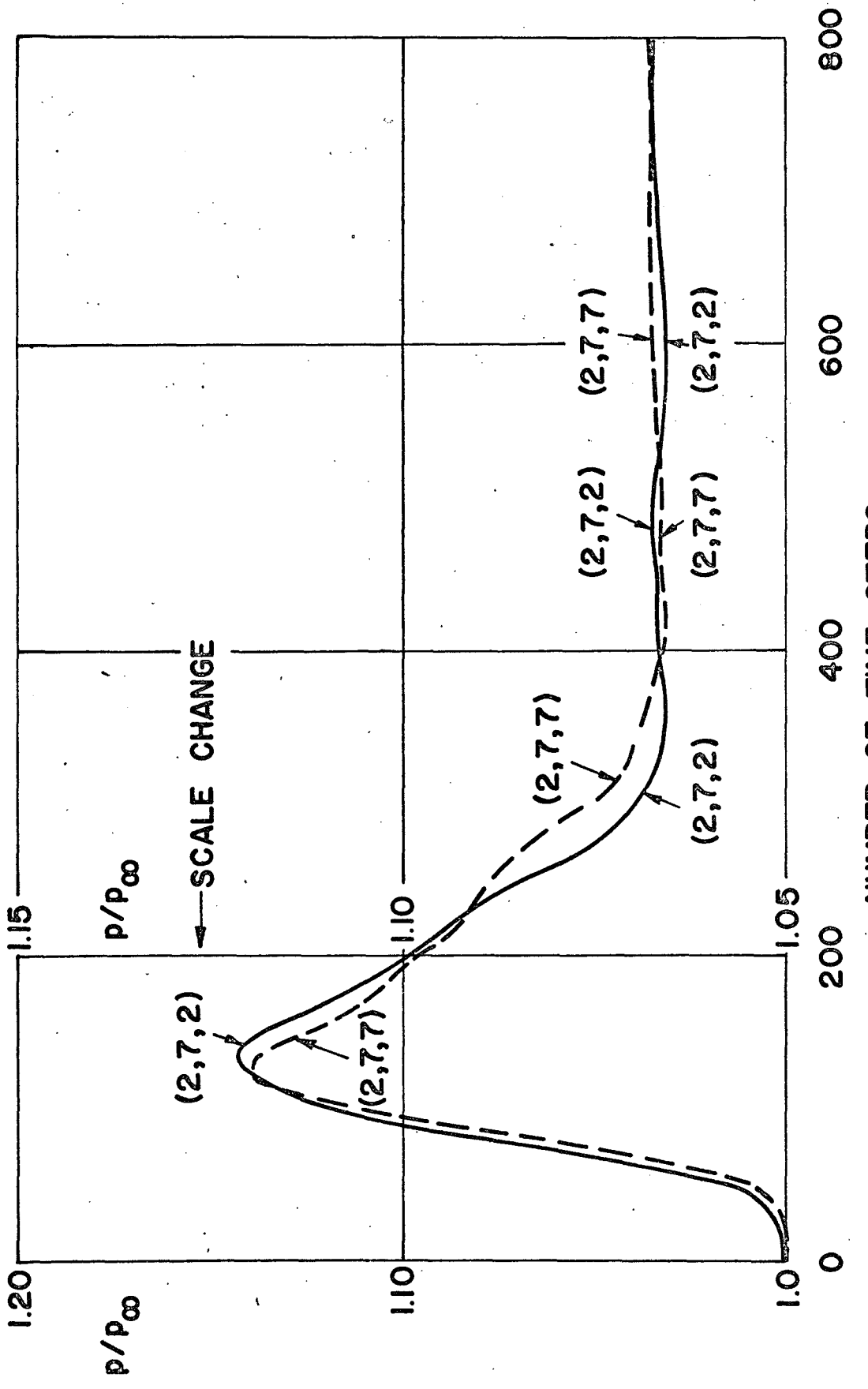

FIGURE 17. PRESSURE VARIATION AT POINTS (2,7,2) AND (2,7,7) UPSTREAM

tions, after the initial starting transient, have a much smaller amplitude and have a frequency of about 1/5 that of the downstream variations. The amplitude of the upstream running waves is reduced by the imbedded supersonic region which causes reflection of the upstream travelling signals from the rotor and by the generally higher Mach number in the region between the stator blades. The peripheral (Y) and axial (X) force variations on the stator blades, shown in Figure (18), also occur at this lower frequency, since less than 1/4 of a cycle appears over 80 time steps. A more extensive coverage of the axial (X) force variations of both sets of blades is presented in Figure (19). A comparison of the frequencies reveals a ratio of about 1/5 between them. The solid portions of the curves are from results at every time step whereas the dashed lines are inferred from the pressure variations on the blade such as the ones shown in Figure (20), and the indicated data points.

The observed ratio of 1/5 in the frequency is a consequence of the particular flow conditions selected for this case, and can be explained as follows: consider a disturbance emitted with a particular wave length λ. The ratio of the signal speed c to frequency f will be the same as the disturbance travels upstream and downstream with the given wave length:

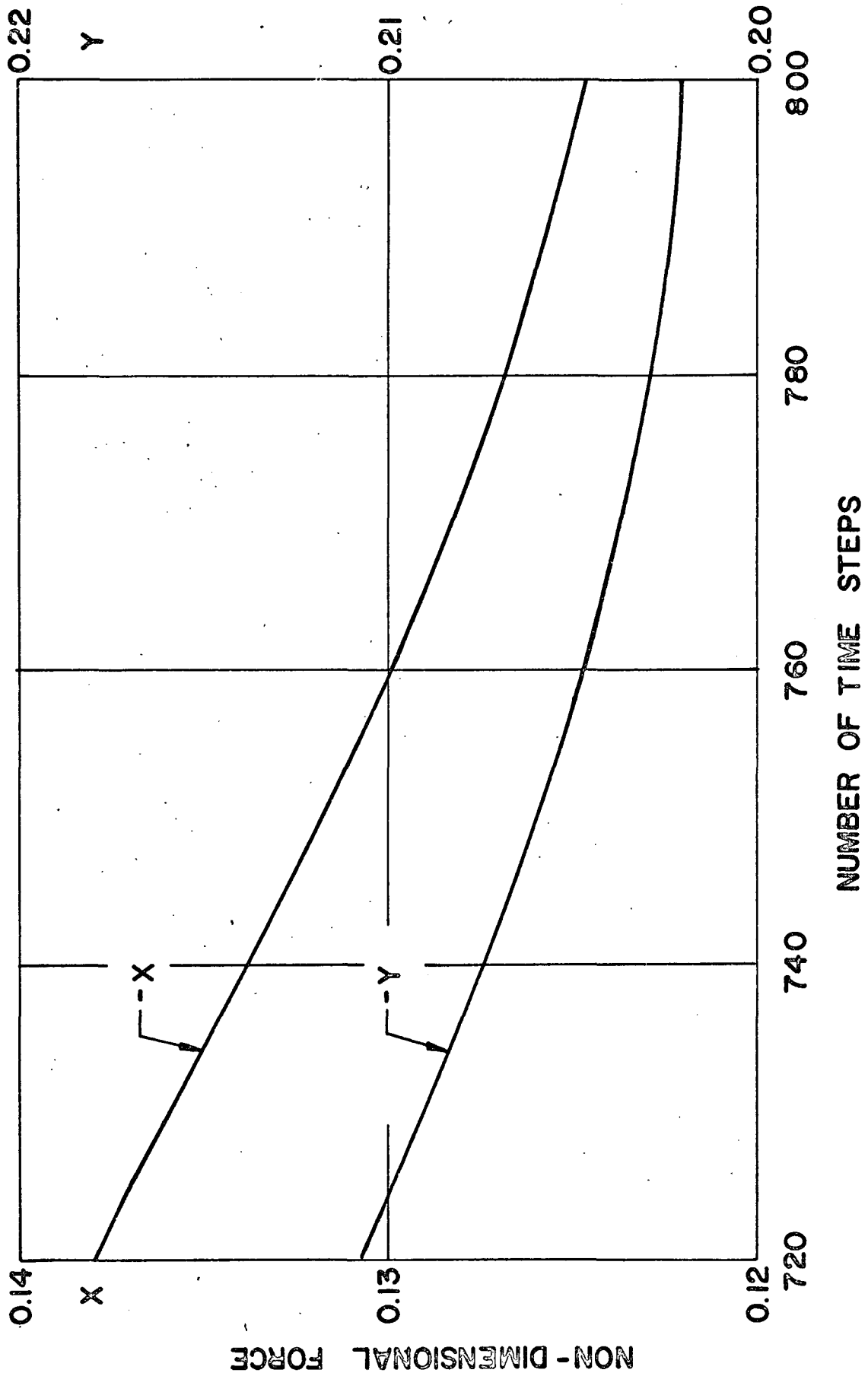

FIGURE 18. PERIPHERAL (Y) AND AXIAL (X) FORCE ON STATIONARY BLADES

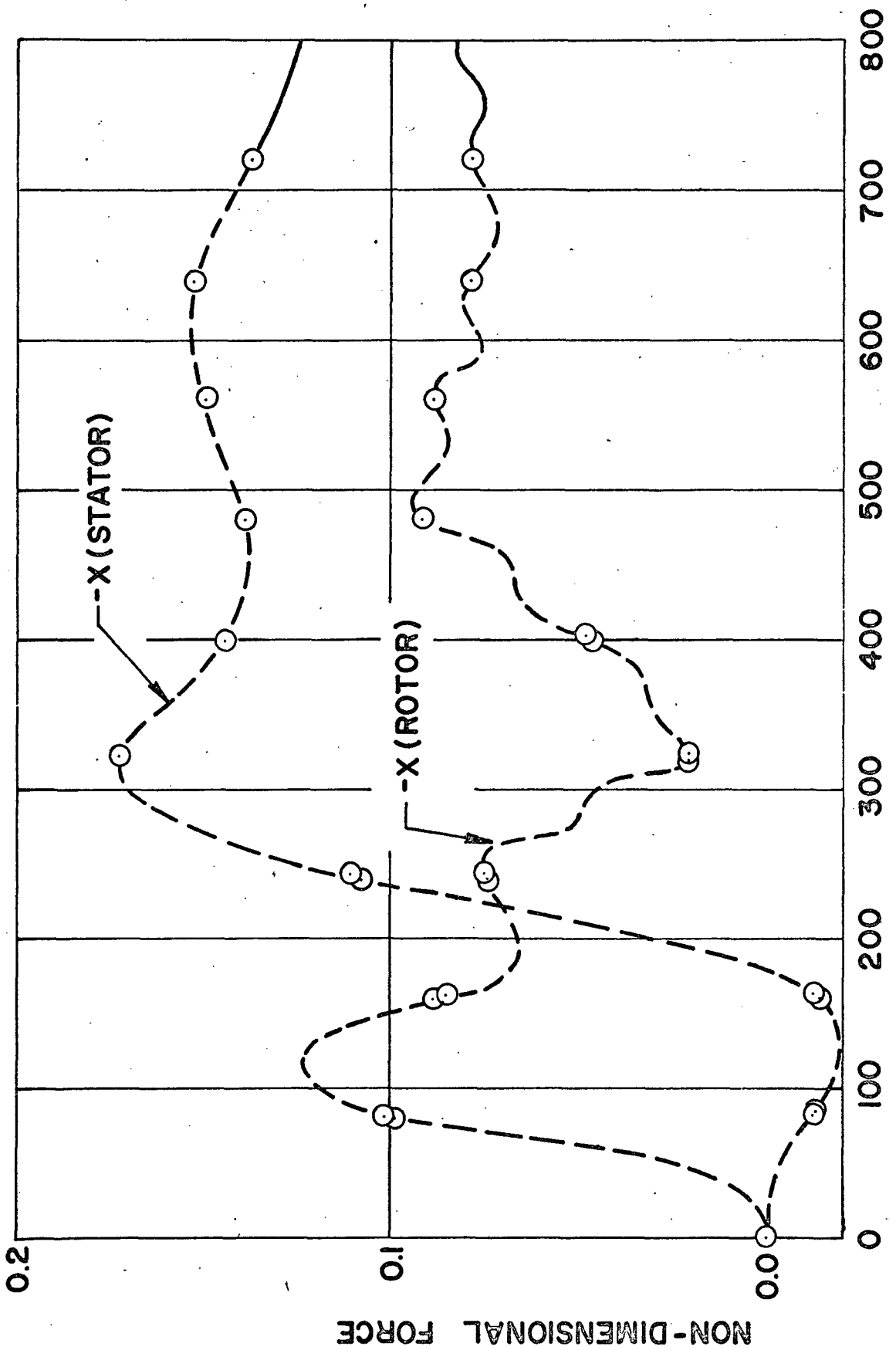

FIGURE 19. AXIAL FORCE VARIATION OF STATOR AND ROTOR BLADES

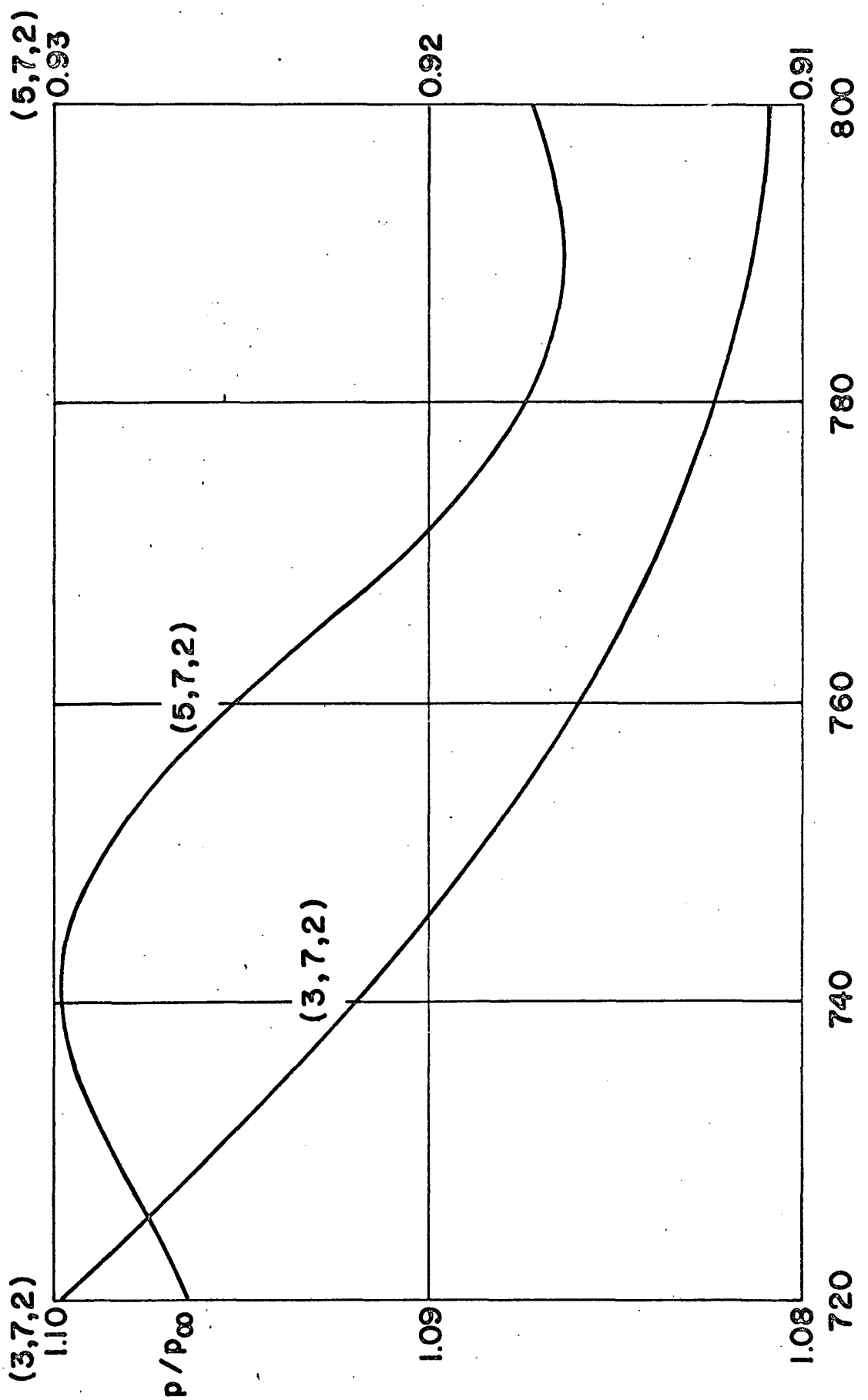

FIGURE 20. PRESSURE VARIATION ON BLADE UPPER SURFACES AT MID CHORD

$$\frac{c_u}{f_u} = \frac{c_d}{f_d} \tag{41}$$

where u refers to upstream and d to downstream.

Therefore,

$$\frac{f_u}{f_d} = \frac{c_u}{c_d} = \frac{a-u}{a+u} = \frac{1-M}{1+M} \tag{42}$$

and since the free stream Mach number, M, is 0.65,

$$\frac{f_u}{f_d} = \frac{.35}{1.65} = \frac{1}{4.72} \simeq \frac{1}{5} \tag{43}$$

One other result of interest is the pressure variation behind the rotor relative to a stationary point. Figure (21) shows such a variation. The fact that the pressure does not return to its original value after one cycle of 80 time steps is an indication that the reflections from the supersonic region are introducing another characteristic frequency or time scale in addition to the fundamental scale given by the blade passing frequency.

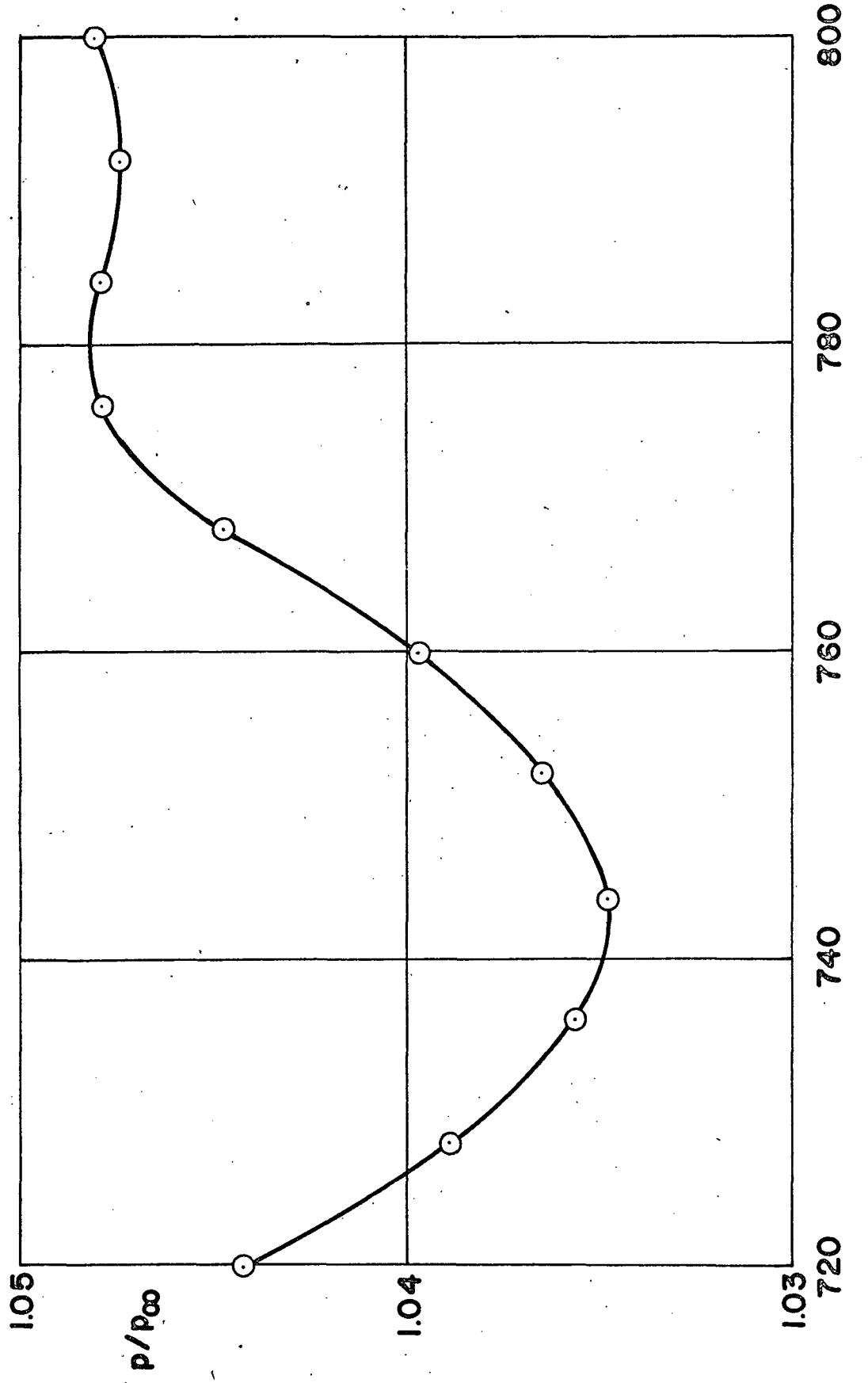

FIGURE 21. SAMPLE PRESSURE VARIATION OBSERVED BY A STATIONARY OBSERVER BEHIND THE ROTOR

IV. CONCLUSIONS

Application of the non steady Lax-Wendroff technique to problems with asymptotically periodic solution offers a potentially powerful method for the investigation of the interaction of rotating and stationary blade rows in turbo-machinery. A novel technique for specifying boundary conditions with phase lag has been developed to accomplish this. A complete non-linear analysis is carried out numerically to determine the entire flow field without recourse to the assumption of small disturbances or linear equations which underlie the previous acoustic theories. The result, obtained for the case of equal number of rotor and stator blades show that transonic flow can be handled without difficulty. In addition, the program is not limited with regard to blade thickness, camber or loading. Extension of this method to incorporate viscous wakes and to analysis of fully three dimensional configuration is feasible, and would greatly expand its utility in practical applications.

REFERENCES

1. Kramer, J. et.al, "Noise Reduction," Chapter VI of Aircraft Propulsion, NASA SP-269, (1970).

2. Rice, G., Feiler, C., and Acker, L., "Acoustic and Aerodynamic Performance of a 6-Foot Diameter Fan for Turbofan Engines, III - Performance with Noise Suppressors," NASA TN D-6178, February 1971.

3. Hartmann, M., et. al., "Fan And Compressor Technology," Chapter I of Aircraft Propulsion, NASA SP-259, (1970).

4. Schorr, R. and Reddy, K., "Inviscid Flow Through Cascades in Oscillatory and Distorted Flow," AIAA Journal 9, 10. pp. 2043-2050, (1971).

5. Okurounmu, O. and McCuna, J., "Three Dimensional Vortex Theory of Axial Compressor Blade Rows at Subsonic and Transonic Speeds," AIAA Journal, 8, 7, pp. 1275-1283, (1970).

6. Lordi, J., "Report on a Study of Noise Generation by a Rotating Blade Row in an Infinite Annulus," Cornell Aeronautical Laboratory, Inc., Report CAL No. AI-2836-A-1, May 1971. Also see Proceedings of NASA Contractors Meeting on Aeronautical Fluid Mechanics, June 1971.

7. Kemp, N. and Sears, W., "Aerodynamic Interference Between Moving Blade Rows, : Jour. Aero. Sci., 20, 9, pp. 585-597, (1968).

8. Mani, R., "Compressibility Effects in the Kemp-Sears Problem," presented at the International Symposium on the Fluid Mechanics and Design of Turbomachinery, Pennsylvania State Univeristy, August 31 - September 3, 1970.

9. Richtmyer, R. and Morton, K., "Difference Methods for Initial Value Problems," 2nd Edition, Chapter 13, Interscience Publishers, New York, (1967).

10. Erdos, J. and Zakkay, V., "Inviscid Solution of the Steady Hypersonic Near Wake by a Time-Dependent Method," AIAA Journal, 9, 7, pp. 1287-1293, (1971).

11. Lighthill, M., "Higher Approximations," Chapter E, Vol. VI of Princeton Series. General Theory of High Speed Aerodynamics, Sear, W., (Editor) Princeton Univ. Press, Princeton, N.J., (1954).

REFERENCES (Continued)

12. Hartree, D.R., "On an Equation Occurring in Falkner & Skan's Approximate Treatment of the Equations of the Boundary Layer," Cambridge Phil. Soc., Vol. 33, Pt. 2, April 1937, pp. 223-239.

13. Schlichting, H., "Boundary Layer Theory," Fourth Edition McGraw-Hill, p. 139 or p. 358, (1960).

14. Ibid, p. 356 or p. 570.